

The Cytotoxicity Induced by Small Gold Nanoparticles: Obtaining the  
Full Picture from Hemolysis, Membrane Deformability, and Blocked  
Endocytosis

By

Hamza Abdel Karim

A thesis submitted to the

Department of Chemistry and Biochemistry

Mount Allison University

in partial fulfillment of the requirements for the

Bachelor of Science degree with Honours in Biochemistry

April 13th, 2023

## Abstract:

The safe application of nanoparticles (NPs) in biomedicine hinges on our full understanding of nanotoxicity. Although small nanoparticles are thought to induce their toxic effects by forming pores in plasma membranes, contradictory results are often encountered in the literature highlighting the intracellular toxicity caused by small NPs. This study resolves the controversy surrounding the topic by blocking endocytosis and examining the toxicity induced by small gold and silver nanoparticles attached to ligands with different hydrophobicities. For the first time, cell lysis and membrane characteristics of brook trout red blood cells are examined in a single statistical analysis to understand their correlation. The results indicate that small NPs induce cytotoxicity intracellularly and that damaging interaction with the membrane is at least partially caused by intracellular pathways. This would open the doors for new delivery techniques of NPs that are accompanied by endocytic inhibitors to decrease their toxic side effects.

## Table of Contents

Abstract .....	2
Table of Contents .....	3
List of Abbreviations.....	4
<b>Introduction</b> .....	5
Applications of Nanoparticles: Why to Study Nanotoxicity .....	5
Characterization of Nanoparticles .....	7
Colchicine and Nanoparticles Uptake .....	8
Trout Erythrocytes and Membrane Deformability.....	10
Experimental Objectives .....	12
<b>Materials and Methods</b> .....	14
Blood Sampling .....	14
Isolation of Red Blood Cells.....	14
Osmotic fragility .....	15
Synthesis and Characterization of Nanoparticles .....	16
Why Should not We be Concerned with Spectral Interference from Colchicine?.....	17
Hemolysis of RBCs with NPs and Colchicine .....	18
Membrane Deformability of RBCs with NPs and Colchicine.....	19
Statistical Analyses .....	20
<b>Results</b> .....	22
Osmotic Fragility of RBCs .....	23
Characterization of NPs .....	24
The effect of NPs and Colchicine .....	25
<b>Discussion</b> .....	39
MANOVA Conclusions .....	39
ANOVA Concluions.....	40
Biological Interpretations and Future Directions .....	42
Acknowledgements .....	46
<b>References</b> .....	47
<b>Appendix</b> .....	54
Absorption Spectra of the Gold Nanoparticles.....	54
Dynamic Light Scattering Results of Nanoparticles .....	55
Raw Data .....	58

## List of Abbreviations

AgPVP	Nanoparticles with silver core protected with polyvinylpyrrolidone
ANOVA	Analysis of Variance
COOH	Undecanoic Acid
DMAP	4-(N, N-Dimethylamino)pyridine
hRBC	Human Red Blood Cell
CaCl <sub>2</sub>	Calcium Chloride
HEPES	4-(2-Hydroxyethyl)-1-Piperazineethanesulfonic Acid
KCl	Potassium Chloride
MANCOVA	Multivariate Analysis of Covariance
MANOVA	Multivariate Analysis of Variance
MgSO <sub>4</sub>	Magnesium sulfate
MS222	Tricane Methanesulfonate
NaCl	Sodium Chloride
NaHCO <sub>3</sub>	Sodium Bicarbonate
NaH <sub>2</sub> PO <sub>4</sub>	Sodium Dihydrogen Phosphate
NP	Nanoparticle
nRBC	Nucleated Red Blood Cell
PVP	Polyvinylpyrrolidone
RBC	Red Blood Cell
ROS	Reactive Oxygen Species
TMAB	Trimethylammonium Bromide

## Introduction:

Nanotechnology is an ever-developing field that aims to employ microscopic, usually 1-100 nm, structures in different applications like cosmetics, medicine, energy and electronics. Although nanoparticles have already been exploited in various fields, there is still much to know about their side-effects, especially from environmental and human health perspectives. In medicine, the ability to apply nanotechnology majorly relies on the safety of such applications. Thus, there has been an absolute need to invest money, time, and effort to establish major themes in nanotoxicology. The latter included defining nanoparticles' distribution in the environment and their ways of interaction with biota. Yet, the major themes seem to partially collapse by the variable and non-systematic guidelines followed by researchers leading to confusion and somewhat controversial data (Carnovale et al., 2019). The controversy stems from examining nanotoxicology without controlling for the numerous variables affecting interaction with biota (Carnovale et al., 2019). That said, nanotoxicology research requires systematic step-by-step investigations on the mechanism of action of nanoparticles.

## **Applications of Nanoparticles: Why to Study Nanotoxicity?**

Nanoparticles come in various structures, shapes, sizes, and surface charges (Mitchell et al., 2021). Figure 1 presents the main structures of nanoparticles and their characteristics. Lipid-based nanoparticles became very familiar as they are used for mRNA delivery in Moderna and Pfizer-BioNTech Covid-19 vaccines (Hou et al., 2021). However, other lipid-based nanoparticles have been previously used in pharmaceuticals like Vyxeos®, a liposome containing DNA polymerase inhibitor, that was FDA approved in 2017 for treatment of acute myeloid leukemia (Blair, 2018). Polymeric nanoparticles are also used in pharmaceuticals, like Abraxane® that is made of an albumin network and used to treat some types of cancers (Green et al., 2006). Unlike

lipid-based nanoparticles, polymeric nanoparticles can have the payload attached on the surface beside being encapsulated within the core (Mitchell et al., 2021). Despite being generally biocompatible and water soluble, they are more likely to aggregate than other nanoparticles (Mitchell et al., 2021), which limits their beneficial role in drug delivery.

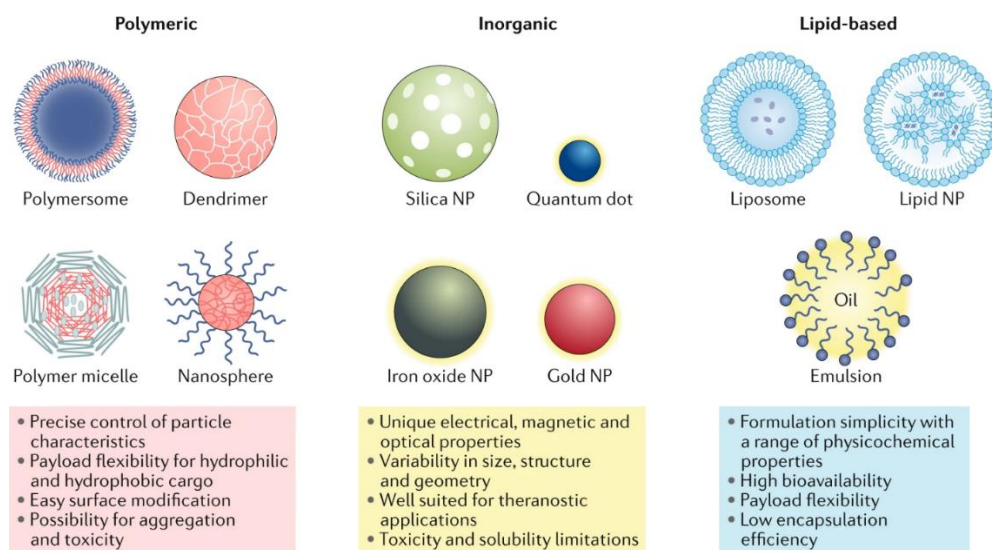


**Figure 1.** Main classes of nanoparticles. Image adopted from (Mitchell et al., 2021).

Inorganic nanoparticles can be precisely engineered to have certain sizes, shapes, and ligands (Mitchell et al., 2021). The metallic nature of gold and silver nanoparticles, despite being sometimes potentially toxic or immunogenic, are beneficial in various applications. Gold nanoparticles are promising tools in diagnostics (Drygin et al., 2009), photothermal therapy of cancer cells (Hirsch et al., 2003) and drug delivery (Yafout et al., 2021). The first clinical use of gold nanoparticles in photothermal therapy was done in 2019, where near infrared laser was used for ablation of prostate cancer and was 94% successful (Rastinehad et al., 2019). The surgery was done following a study that examined the effects of the same gold nanoparticles on patients with prostate cancer who later had radical prostatectomy (Stern et al., 2016). Even in

immunology, gold nanoparticles can elicit a full immune response when loaded with antigens with no need for further adjuvants, probably due to their potential in stimulating immune responses as adjuvants by themselves (Mateu Ferrando et al., 2020). That said, to both optimize their use and mitigate unintended consequences, the inherent toxicity of NPs must equally be understood.

Meanwhile, silver nanoparticles have witnessed broader non-invasive applications because of their antibacterial activity (X. Chen & Schluesener, 2008). For instance, dressings and sutures coated with silver nanoparticles have been clinically approved (X. Chen & Schluesener, 2008). This was despite the debate over their possible cytotoxicity and leakage to circulation via subcutaneous lymphatic vessels. Overall, despite approving some gold and silver nanoparticles, there is little consensus on their safety upon their entrance to tissues and interactions with cells, which makes the topic of nanotoxicology an extreme necessity for full optimization of nanoparticles applications. As mentioned previously, nanoparticles have several characteristics beside their structural material, like charge or shape, and the first step into optimization of NPs is the comprehension of the origin and consequences of such characteristics. These are summarized in the next section.

### **Characterization of Nanoparticles**

Any examination of nanotoxicity requires knowledge of broad characteristics of the investigated nanoparticle. The characteristics can be summarized as: size, shape, charge and surface coatings (Mitchell et al., 2021). While the shape and ligands can be entirely determined by the synthesis procedures, the size and charge are greatly affected by the solution in which nanoparticles are used. There is a great variety of sizes ranging from 1 nm to 100 nm or even above (Mitchell et al., 2021). Groups of nanoparticles with a specific size range tend to behave

similarly in their interaction with biota (Mitchell et al., 2021). For instance, polar nanoparticles smaller than 22 nm in diameter are thought to form pores in lipid membranes (Roiter et al., 2008). Meanwhile, larger nanoparticles tend to be enveloped into the membranes initiating an endocytic pathway (Roiter et al., 2008). In this study only NPs with a core size of ~ 5 nm are applied which are expected to exert their effects extracellularly on the plasma membrane.

It is important to note, however, that the diameter size of a nanoparticle is not merely the core size or the ligand-conjugated core size. When in solution, a single nanoparticle along with its ligands attract molecules from the solution, like ions and water molecules. As a result, the size of a nanoparticle in solution is most often larger than its actual core size (Jiang et al., 2009). Thus, the term hydrodynamic diameter, which takes into consideration this effect, better represents the actual size of the nanoparticle in solution (Jiang et al., 2009). Here, All NPs applied tend to have a hydrodynamic diameter less than 22 nm.

Surface charge also has a distinct terminology in nanotechnology because of the molecules attracted to the nanoparticle's surface. Assuming no attraction, one would only consider the charge of the ligands and the oxidation state of the surface metal molecules. However, because of the molecules attracted to the surface, it is essential to consider the potential difference between the innermost and outermost molecules in the electrical double layer (ligands and attracted molecules) surrounding the nanoparticle (Jiang et al., 2009). Such potential is referred to as the zeta potential (Jiang et al., 2009), which represents the actual charge of the nanoparticle that will direct its biological behavior.

### **Colchicine and Nanoparticles Uptake.**

Colchicine is a popular molecule that gained reputation from its *in vitro* anticancer potential (Z.-Y. Lin et al., 2016). The molecule is clinically accepted for treatment of gout arthritis within a plasma concentration range of 2-6 ng/mL (Dhyani et al., 2022). It exerts its actions by preventing microtubule assembly and thus interfering with microtubule-based chemotaxis, generation of cytokines, and phagocytosis in immune cells (Dalbeth et al., 2014). Its antitumor potential arises from the same mechanism; it binds to tubulins (the building blocks of microtubules) and disrupts the formation of the mitotic spindle (Dhyani et al., 2022), according to figure 2.

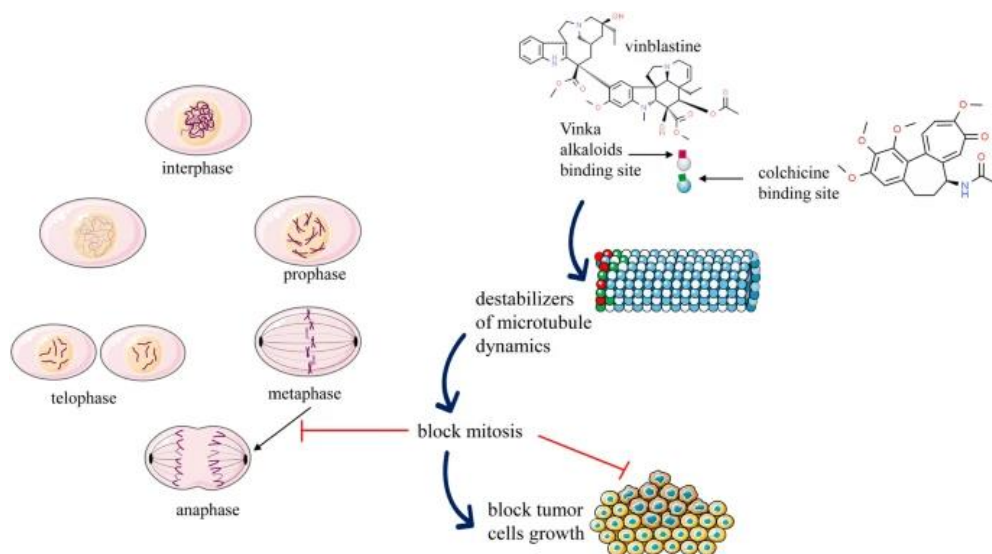


**Figure 2.** Colchicine destabilizes microtubules interfering with mitosis. Image adopted from (Dhyani et al., 2022)

Disruptions in microtubules also affect the structure of cellular organelles causing disorganization of Golgi apparatus (Piasek & Thyberg, 1979), which leads to impaired endocytosis (Tang et al., 2017). While endocytosis has multiple routes, colchicine seems to disrupt all the routes non-specifically which is supported by their mechanism of action that impedes intracellular trafficking. In addition, it has been shown to inhibit pinocytosis (Nilsson et

al., 1983) and clathrin-mediated endocytosis (Kitchens et al., 2008). Also, caveolar-mediated endocytosis (Mundy et al., 2002) and macropinocytosis (Kruth et al., 2005) have been shown to be dependent on microtubules besides actin, which suggests that colchicine is a potent inhibitor of these pathways. Such an effect has been exploited to understand whether endocytosis is the dominant uptake pathway of certain functionalized-nanoparticles (I.-C. Lin et al., 2012). Here, colchicine is exploited to understand the mechanism of toxicity by impeding the entry of nanoparticles into red blood cells and observing the toxicity caused by the extracellular nanoparticles.

### **Trout Erythrocytes and Membrane Deformability**

Nanotoxicity with human red blood cells (hRBCs) provides potent examination of nanoparticles effect on human health upon intravenous introduction. However, hRBCs are not optimal for understanding the mechanism of toxicity because their mechanism of nanoparticle uptake is not fully understood (Zhao et al., 2011). Human erythrocytes can be young or old RBCs (Matovcik et al., 1985), and differ in their endocytic abilities. Also, neonatal hRBCs (drawn from the umbilical cord) differ from adult hRBCs (Matovcik et al., 1985). Neonatal hRBCs exhibit more frequent endocytic vacuoles and can perform receptor-mediated endocytosis that is absent in adult hRBCs (Matovcik et al., 1985). More importantly, in adult and neonatal hRBCs, young RBCs show better response to membrane active agents that induce endocytosis (Matovcik et al., 1985). Apparently, the endocytic performance of hRBCS is not well understood, which undermines its role as a model to understand nanotoxicity.

The poor endocytosis in hRBCs has been mistakenly stereotyped to the RBCs of other species. L. Q. Chen et al. (2015) assumed the absence of phagocytosis in Goldfish RBCs (*Carassius auratus*) and concluded that other modes of uptake dominate nanoparticles

intracellular toxicity. Nevertheless, phagocytosis has been shown to occur in the nucleated RBCs (nRBCs) of bony fish (Qin et al., 2019), along with adaptive immune activity (Stosik et al., 2020). Such a settled difference between hRBCs and nRBCs not only implies a difference in how different organisms initially respond to nanoparticles, but also highlights nRBCs as a potent cellular model to study nanotoxicity.

Trout RBCs are nRBCs that have been previously shown to exhibit phagocytosis (McLeese & Eales, 1996). Moreover, brook trout (*Salvelinus fontinalis*) blood cell profile (cell types) is very similar to the mammalian profile with differences in count, shape, and morphology (Suljević & Mitrašinović-Brulić, 2020). While hRBCs are cylindrical (Nash & Egginton, 1993), nRBCs of brook trout are oval with elongated nuclei (Suljević & Mitrašinović-Brulić, 2020). Previous examination of a different trout species, rainbow trout (*Oncorhynchus mykiss*), revealed that in comparison to the cylindrical hRBCs with a diameter of 8  $\mu\text{m}$ , the oval nRBCs of rainbow trout are 16, 11.5, and 2.5  $\mu\text{m}$  in length, width, and thickness, respectively (Nash & Egginton, 1993).

Both cell types need to pass through capillaries that can reach 3  $\mu\text{m}$  in diameter (Nash & Egginton, 1993), which means that cells need to adopt a new shape by deforming their membranes. Figure 3 illustrates the idea of membrane deformability, where a rainbow trout nRBC (in 1A) is being aspirated into a micropipette with a diameter of 3.1  $\mu\text{m}$  (in B). The deformability can be quantified in various ways. Nash and Egginton (1993) expressed deformability by measuring the length of the aspirated membrane tongue (shown in figure 3 B) in response to a specific pressure. Reid et al. (1976) quantified deformability by the term deformability index. Which is expressed as the volume of RBCs passed through a nucleopore filter (with a pore diameter of 5  $\mu\text{m}$ ) in one minute, at a specific pressure. The latter

quantification is practical and has been applied to study the effect of nanoparticles on hRBCs (Zhao et al., 2011). Thus, the effect of nanoparticles on membrane deformability can be quantified.

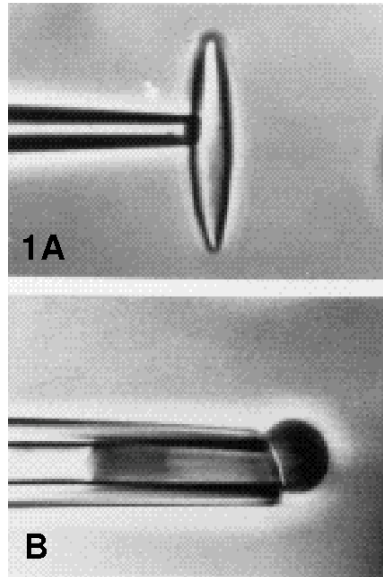


**Figure 3.** Aspiration of a rainbow trout (*Oncorhynchus mykiss*) red blood cell into a pipette with 3.1  $\mu\text{m}$  in diameter. 1A) the trout RBC before aspiration. B) the trout RBC is being aspirated by squeezing a membrane tongue into the pipette. Image adopted from (Nash & Egginton, 1993).

### Experimental Objectives

The experimental approach followed in this research adopts the previous suggestion by Carnovale et al. (2019) to have a systematic experimental design in which size, charge or surface ligands should be controlled, which would help constitute a pattern of toxicity. Here, the core size of NPs is chosen to be 5 nm and the hydrodynamic diameter is controlled to be below 20 nm to test for the extracellular interaction with cell membranes. The cells used are brook trout nRBCs that form a good model to study nanotoxicity as they have nuclei, perform phagocytosis, and lack paracellular pathways.

Ligands with different hydrophobicity are attached to gold nanoparticles to test for hydrophobicity-dependent membrane interaction. Also, one type of silver nanoparticles is added to the analysis to control for the core size and compare toxicity of gold nanoparticles to a model nanoparticle that shows concentration-dependent toxicity. Upon addition of colchicine to nRBCs, nanoparticles are forced to interact with the membranes extracellularly, as endocytosis is inhibited. After exposure to osmotic stress, the cells swell and lyse, with lysis being proportional to the ability of nanoparticles to interact with cell membranes and disturb their integrity. As a result, a pattern of toxicity is established that depends on the hydrophobicity and zeta potential of nanoparticles by having the size constant. By measuring membrane deformability after exposure to different nanoparticles, a relationship is established between hemolysis and membrane interaction to examine whether toxicity is induced at the level of the plasma membrane.

The main hypothesis in this study is that the small NPs will form pores on the membranes and cause lysis in a ligand hydrophobicity-dependent manner. This general hypothesis can be divided into smaller hypotheses to make it more easily testable by linking it with the experimental design. First, NPs will cause toxicity (an increase in hemolysis and a decrease in membrane deformability) that is proportional to the ligand hydrophobicity, with more hydrophobic ligands causing NPs to be more toxic. Second, blocking endocytosis will increase hemolysis because the small NPs in this study are expected to interact extracellularly with the membrane. Finally, blocking endocytosis should not affect membrane deformability as NPs are supposed to be acting extracellularly.

## Materials and Methods:

**Blood Sampling.** Brook trout (*Salvelinus Fontinalis*) were anesthetized in a water bucket with 0.1 g/L Syncaine (MS222) buffered with 0.2 g/L sodium bicarbonate. The volume of the water was slightly increased according to the size of the fish with a minimum volume of 5 L. The fish were left until gill movement ceased (typically after 15 minutes), meanwhile the fish were constantly swirled around the bucket to ensure enough oxygenation. Later the fish were quickly placed dorsal side up and blood was drawn with 100 U/mL heparinized 21-gauge needle at approximately 1 cm below the adipose fin. Sampled fish were tagged with a tagging gun on their dorsal fins and were left to recover with no sampling for at least two weeks (Lawrence et al., 2020). Fish were then quickly returned to their original tanks and swished back and forth until they were able to swim.

The hematocrit of the blood was determined by emptying 150  $\mu$ L of blood onto a parafilm. Then, blood was drawn into two capillary tubes (FisherBrand™ Microhematocrit Capillary Tubes) that were centrifuged for 5 minutes at 2380 RCF (GCH-24 Hematocrit Centrifuge, globe scientific INC.). A ruler was used to measure the ratio of the height of the red column relative to the entire height of the blood sample after centrifugation. The % hematocrit was then determined from multiplying the ratio by 100.

**Isolation of Red Blood Cells.** Blood was emptied from the syringe into 10 mL falcon tubes such that each tube receives 1 mL of blood. Followed by the addition of 9 mL isolation saline (142 mM NaCl, 0.90 mM MgSO<sub>4</sub>, 3.35 mM KCl, 2.30 mM NaH<sub>2</sub>PO<sub>4</sub>, 5.50 mM NaHCO<sub>3</sub>, 10 mM HEPES, 5.0 mM D-glucose, and 100 U/mL of heparin). The tubes were then centrifuged at 500 RCF for 8 minutes (at 10 °C), the supernatant was pipetted out, and the cell pellet was resuspended with the appropriate volume of isolation saline to reach 10 mL. This step was

repeated multiple times so that a total of 5 washes were achieved. The final cell pellet was re-suspended in the isolation saline so that the hematocrit in the falcon tube totaled 8%. The blood was stored in an ice box placed on a shaker until further experiments were performed (in the range of 2 hours to 48 hours). Nevertheless, each experiment had its own control which was drawn from the storage tube at the same time of the experimental treatments.

**Osmotic Fragility.** RBCs were tested for their osmotic fragility by exposing them to various solutions of the isolation saline each with a different NaCl concentration. After isolation of RBCs, they were transferred into different Eppendorf tubes containing the isolation saline with the appropriate [NaCl] so that the final hematocrit treated is 1%. The [NaCl] tested (in mM) were 0, 20, 40, 60, 90, 120, and 143. One of the tubes contained only ddH<sub>2</sub>O with no salts and is referred to as the negative control because RBCs are expected to fully lyse in it. Meanwhile, the 143 mM solution is referred to as the positive control where RBCs are not expected to lyse. The tubes were mixed on ice for 30 minutes on an orbital shaker and later centrifuged at 1500 RCF and 4 °C for 5 minutes using Eppendorf 5424 Centrifuge (Eppendorf, Hamburg, Germany). The absorbance of the supernatant (V = 200 μL) was measured at 570 nm using Spectra Max 190 microplate spectrophotometer (Molecular Devices, US). The % hemolysis was calculated as previously suggested (L. Q. Chen et al., 2015) from the following equation (equation 1):

$$\% \text{ Hemolysis} = \frac{(\text{sample absorbance at 570 nm}) - (\text{absorbance of positive control at 570 nm})}{(\text{absorbance of negative control at 570 nm}) - (\text{absorbance of positive control at 570 nm})} \times 100$$

Data were plotted using GraphPad Prism 9.4.0 and then were fit in a non-linear [inhibitor] vs normalized response curve. This type of curve best represents the data as protein activity can be replaced by % hemolysis and the inhibitor can be replaced with [NaCl]. However,

no conclusions are drawn from the fit parameters and the nature of this fit is only exploratory that aims to estimate  $R^2$ .

**Synthesis and Characterization of Nanoparticles (NPs).** 4-(N, N-Dimethylamino)pyridine-Protected nanoparticles with a 5 nm core size were obtained (Bryan S, Mount Allison University). Ligand exchange of the desired ligands was performed on the DMAP NPs as previously described (Rucareanu et al., 2006). The desired ligand thiol was added to 40 mL of DMAP NPs and 60 mL of water so that its final concentration in the reaction RBF is 0.45 mM. When the ligand is in the solid state, it is first dissolved in water and then added to 40 mL of DMAP NP solution. The solution was stirred overnight and later separated by size-exclusion chromatography using using Sephadex® LH-20 column with water as the eluting medium to eliminate unbound surfactant. To enhance the purity of NPs, eluted solutions were added to 30K Macrosep® Advance Centrifugal Devices (PALL® corporation, US). These were centrifuged at 12,000 g for 30 minutes, the eluant was discarded and the filtered solution contained the NPs. The nanoparticles in this study are attached to the following ligands: mercaptoundecanoic acid (COOH), mercaptopropionic acid (MPA), polyvinylpyrrolidone (PVP), and (11-mercaptoundecyl)-N,N,N-trimethyl ammonium bromide (TMAB). Commercially available silver nanoparticles of the same core size (5nm) and ligated with PVP (AgPVP) were purchased (lot # MPOO42, nanoComsix, Canada) and used as a control for concentration-dependent toxicity.

Characterization of NPs was done using Malvern Zetasizer (Malvern Panalytical, UK). Solutions of purified NPs were first diluted with ddH<sub>2</sub>O (1:5), run through 0.4 µm filters, and then added to folded capillary zeta cells (Malvern Panalytical, UK) to perform the analysis. The concentrations of NPs were determined using a previously established spectrophotometric method (Haiss et al., 2007). Solutions of NPs (V= 200 µL) were added to a microplate and the

absorbance spectra for each NP was determined using SpectraMax 190 (Molecular Devices, US). First, the wavelength at which surface plasmon resonance occurs was verified to be around 520 nm for 5nm gold NPs. Then, the core size of the NPs was assured by determining the ratio of absorbance at the surface plasmon peak to the absorbance at 450 nm and comparing it to previously established ratios (Haiss et al., 2007). After confirming the core size, the absorptivity of NPs at 450 nm is obtained from Haiss et al. (2007). Finally, the concentration of each NP was determined with Beer-Lambert law as follows:

$C = \frac{\text{Absorbance at 450 nm}}{\epsilon (\text{at 450 nm}) \times d}$ , where  $d = 0.4$  cm for the 200  $\mu$ L in microplate. Absorption spectra of the different gold NPs are shown in the Appendix.

**Hemolysis of RBCs with NPs and Colchicine.** Colchicine (Sigma Aldrich) was dissolved in 143 mM of isolation saline (with no glucose or an anticoagulant), the final stored concentration was 2.5 mM and the storage vial was covered with aluminum foil to prevent photodegradation. Before exposing RBCs to NPs, the isolation saline and the NP solutions were added to 1.5 mL Eppendorf tubes so that the final NP concentrations would be 5, 10, or 20 nM at a final volume of 1 mL. Meanwhile, NaCl concentration in all tubes would be 50 mM at a final volume of 1 mL. For RBCs treated with colchicine, the prepared colchicine solution was added to the 1.5 mL Eppendorf tubes along with the isolation saline and the NP solutions. The addition was so that colchicine concentration in all tubes would be 0.5 mM, NaCl concentration would be 50 mM, and NP concentrations would be either 5, 10, or 20 nM at a final volume of 1 mL. A tube containing water only and another containing isolation saline at 143mM NaCl were used as negative and positive controls, respectively.

Freshly isolated RBCs were added to the tubes so that the final hematocrit in each treatment tube is 0.5%. The tubes were shaken on ice for 45 minutes on an orbital shaker and later centrifuged at 5000 *g* and 4 °C for 5 minutes using Eppendorf 5424 Centrifuge (Eppendorf, Hamburg, Germany). The absorbance of the supernatant ( $V = 200 \mu\text{L}$ ) was measured at 570 nm using Spectra Max 190 (Molecular Devices, US). The % hemolysis was calculated from equation 1.

**Why Should not We be Concerned with Spectral Interference from Colchicine?** The absorption spectrum of colchicine is shown in figure 4, where there is a distinct peak at 350 nm, with a tendency to red-shift with protic polar solvents (Ghanem et al., 2010). The other distinct peak occurs at 245 nm (Ghanem et al., 2010). Figure 5 shows the absorption spectrum of colchicine-tubulin complex with the same distinct peak at around 350 nm (Arai & Okuyama, 1975). From these spectra, addition of colchicine is not expected to interfere with the hemoglobin peak at 570 nm that is usually used from hemolytic assays with silver and gold nanoparticles. Therefore, the addition of colchicine should not interfere with the hemolytic assays, assuming colchicine is not binding to other cellular structures and altering absorption patterns. Moreover, the colchicine-tubulin complex has a distinct fluorescence pattern where absorption at 350 nm can lead to fluorescence at 400 nm (Arai & Okuyama, 1975). Something that can be exploited to confirm the binding of the molecule to tubulins causing endocytosis inhibition.

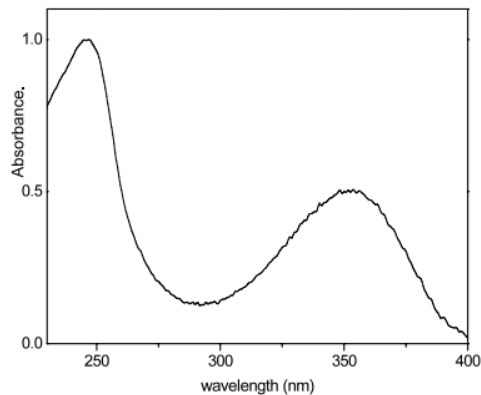


**Figure 4.** Absorption spectrum of colchicine. Image adopted from (Ghanem et al., 2010).

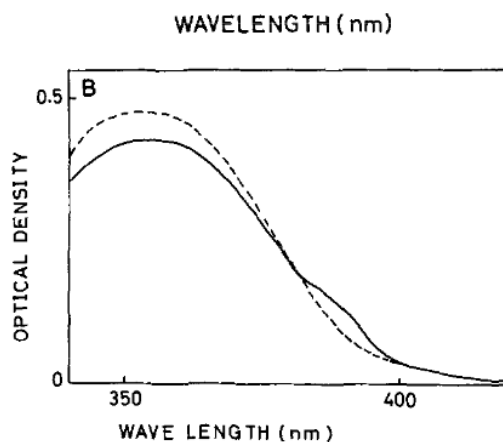


**Figure 5.** The absorption spectrum of colchicine-tubulin complex. Image adopted from (Ghanem et al., 2010).

**Membrane Deformability of RBCs with NPs and Colchicine.** Isolation saline and the NP solutions were added to 1.5 mL Eppendorf tubes so that the final NP concentrations would be 5, 10, or 20 nM at a final volume of 1 mL. Meanwhile, NaCl concentration in all tubes would be 143 mM at a final volume of 1 mL. For RBCs treated with colchicine, the prepared colchicine

solution was added to the 1.5 mL Eppendorf tubes along with the isolation saline and the NP solutions. The addition was so that colchicine concentration in all tubes would be 0.5 mM, NaCl concentration would be 143 mM, and NP concentrations would be either 5, 10, or 20 nM at a final volume of 1 mL. Freshly isolated RBCs were added to the tubes so that the final hematocrit in each treatment tube is 0.5%. The tubes were shaken on ice for 45 minutes on an orbital shaker before starting the assessment of membrane deformability.

Membrane deformability was recorded as a deformability index ( $\text{mL}\cdot\text{min}^{-1}$ ) as established previously (Reid et al., 1976) and explained in the introduction with variations regarding pressure application. The final RBC solution was drawn into a 1 mL syringe (BD, Canada) and inserted into a membrane holder that was stabilized onto a 250-mL Erlenmeyer flask. The membrane holder contained a 5.0  $\mu\text{m}$  mixed cellulose esters (MCE) membrane (Millipore®, Ireland). A mass of 99 g was placed on the syringe to drive the solution across the membrane into the Erlenmeyer flask with a pressure of 12 kPa. Pressure was measured with a transducer (Memscap) calibrated to a static water column and interfaced to a Powerlab 8/35 data acquisition system (ADInstruments) and data was recorded with associated Lab Chart software. The time it took for the full 1 mL solution to get into the flask was recorded and the index was calculated as

$$\text{index} = \frac{V(\text{eluted})}{\text{time}(\text{seconds})} \times \frac{60 \text{ seconds}}{1 \text{ minute}}.$$

Membranes and syringes were changed every fourth trial to ensure membrane blockage and increased friction of the syringe did not affect the measurements.

**Statistical Analyses.** All analyses were done using RStudio (2023). Since 3 concentrations were tested for each NP, the most appropriate analysis to perform is multivariate analysis of covariance (MANCOVA) where the covariate is the NP concentration. Because some of the NPs applied are hydrophobic, there is a high chance that they will aggregate according to their hydrophobicity in the aqueous saline solution. So, there might be an interaction between NP

concentration and the dependent variables and the first assumption that needed to be assessed was homogeneity of regression slopes. This assumption was not met, and MANCOVA could not be performed. Therefore, data were split into 3 datasets each corresponding to one concentration and a MANOVA was performed on each dataset.

For the first concentration (10 nM), data passed univariate homogeneity of variance and homogeneity of covariance matrices. Both univariate and multivariate normality were satisfied and MANOVA was run. The statistical null hypotheses are as follows: the mean of hemolysis across all NP types is the same, the mean of hemolysis is the same with the presence and absence of colchicine, the mean of deformability across all NP types is the same, the mean of deformability is the same with the presence and absence of colchicine, and there is no interaction between NP type and colchicine presence. The results indicated a significant multivariate interaction between NP type and colchicine presence.

Examination of the data with plotting revealed that the interaction is caused by the effect size of colchicine addition, but the effect of colchicine was uniform across all NP types. The examination of the data was followed by post hoc permutational MANOVA on the NP types, and Hotelling's t-test on the effect of colchicine on the individual NPs. In the latter, subsets were generated for each NP with the two dependent variables and the two levels of colchicine factor. Canonical discriminant analysis was later performed and the correlation between the dependent variables was revealed. Finally, univariate analyses were done for each dependent variable.

For the second concentration (20 nM), data passed univariate homogeneity of variance and homogeneity of covariance matrices. While univariate normality was satisfied, multivariate normality was not, and later MANOVA was run. The statistical null hypotheses are as follows: the mean of hemolysis across all NP types is the same, the mean of hemolysis is the same with

the presence and absence of colchicine, the mean of deformability across all NP types is the same, the mean of deformability is the same with the presence and absence of colchicine, and there is no interaction between NP type and colchicine presence. The results indicated a significant multivariate interaction between NP type and colchicine presence. The results indicated a significant multivariate interaction between NP type and colchicine presence.

Just like the first concentration, the interaction is caused by the effect size of colchicine addition, but the effect of colchicine was uniform across all NP types. Post hoc permutational MANOVA on the NP types was done along with Hotelling's t-test on the effect of colchicine on the individual NPs as in the previous concentration. Canonical discriminant analysis was later performed and the correlation between the dependent variables was revealed. Finally, univariate analysis was done for each dependent variable.

For the third concentration (40 nM), data passed univariate homogeneity of variance but did not pass homogeneity of covariance matrices although the latter can be debated due to the marginal p-value. Univariate normality for deformability was not met, meanwhile normality for hemolysis was met. Therefore, deformability data were log 10 transformed, and normality was met after the transformation. Homogeneity of variance and covariance matrices were rechecked, and both were met after the transformation, but multivariate normality was not met. MANOVA was run and the statistical null hypotheses are as follows: the mean of hemolysis across all NP types is the same, the mean of hemolysis is the same with the presence and absence of colchicine, the mean of log 10 deformability across all NP types is the same, the mean of log 10 deformability is the same with the presence and absence of colchicine, and there is no interaction between NP type and colchicine presence. The results indicated a significant multivariate interaction between NP type and colchicine presence.

As in the other concentrations, the interaction is caused by the effect size of colchicine addition, but the effect of colchicine was uniform across all NP types. Post hoc permutational MANOVA on the NP types was done along with Hotelling's t-test on the effect of colchicine on the individual NPs as in the previous concentrations. Canonical discriminant analysis was later performed and the correlation between the dependent variables was revealed. Finally, univariate analysis was done for each dependent variable.

## Results:

### **Osmotic Fragility of RBCs**

Before examining the effect of NPs and colchicine on RBCs, it is beneficial to observe how RBCs respond to osmotic pressure and justify the use of 50 mM NaCl in hemolysis experiments of NPs. Figure 6 illustrates the osmotic fragility of brook trout RBCs in response to decreasing NaCl concentration in the isolation saline. The curve can be best fit with a non-linear regression where NaCl is the inhibitor of the % hemolysis (the normalized response) with an  $R^2$  of 0.81. Such a regression yields an  $IC_{50}$  of  $23 \pm 2$  mM, which suggests that half of the RBCs lyses at  $[NaCl] = 23$  mM after 30-minute exposure on ice. It is noticeable how at  $[NaCl]$  smaller than 50 mM, the RBCs become extremely sensitive to  $[NaCl]$  and any small changes in  $[NaCl]$  cause large changes in % hemolysis. Thus, it is reasoned that RBCs become weak at this osmotic pressure and any small damaging interaction with the membrane by NPs is expected to cause large hemolysis.

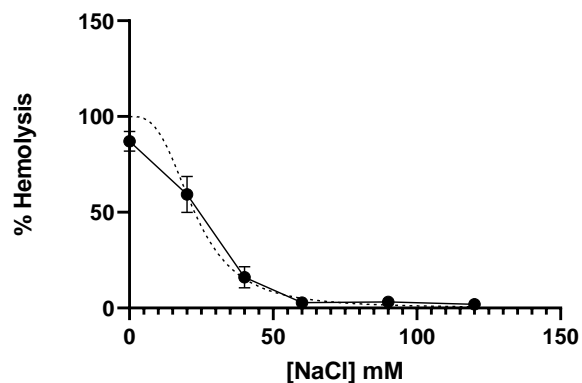


**Figure 6.** Osmotic Fragility of RBCs. The lysis of RBCs in response to various [NaCl] in RBC isolation saline (0.90 mM MgSO<sub>4</sub>, 3.35 mM KCl, 2.30 mM NaH<sub>2</sub>PO<sub>4</sub>, 5.50 mM NaHCO<sub>3</sub>, 10 mM HEPES, 5.0 mM D-glucose, and 100 U/mL of heparin). Eppendorf tubes (1.5 mL) containing the RBC solutions were shaken on ice for 30 minutes on an orbital shaker and later centrifuged at 1500 RCF and 4 °C for 5 minutes using Eppendorf 5424 Centrifuge (Eppendorf, Hamburg, Germany). The absorbance of the supernatant (V = 200 μL) was measured at 570 nm using Spectra Max 190 (Molecular Devices, US). The % hemolysis was calculated from equation 1. Data were plotted using GraphPad Prism 9.4.0 and then were fit in a non-linear [inhibitor] vs normalized response curve (dashed curve) with an R<sup>2</sup> of 0.81.

### Characterizations of NPs

The dynamic light scattering (DLS) results are summarized in figure 7. All nanoparticles have negative zeta potential except for TMAB NPs which have a positive charge of 20 +/- 12 mV. While more than one diameter is detected in all DLS experiments (see supplementary figures), only the smallest diameter is recorded in figure 7. The other diameters are larger than 20 nm resulting from NP aggregation and are not expected to be toxic because of the relatively large size. The hydrophobicity of the ligands is added to DLS results to provide a full overview of the ligands. COOH NPs have the most hydrophobic ligand with a log K<sub>ow</sub> of 4.42, whereas PVP NPs have the least hydrophobic ligand with a log K<sub>ow</sub> of 0.40.

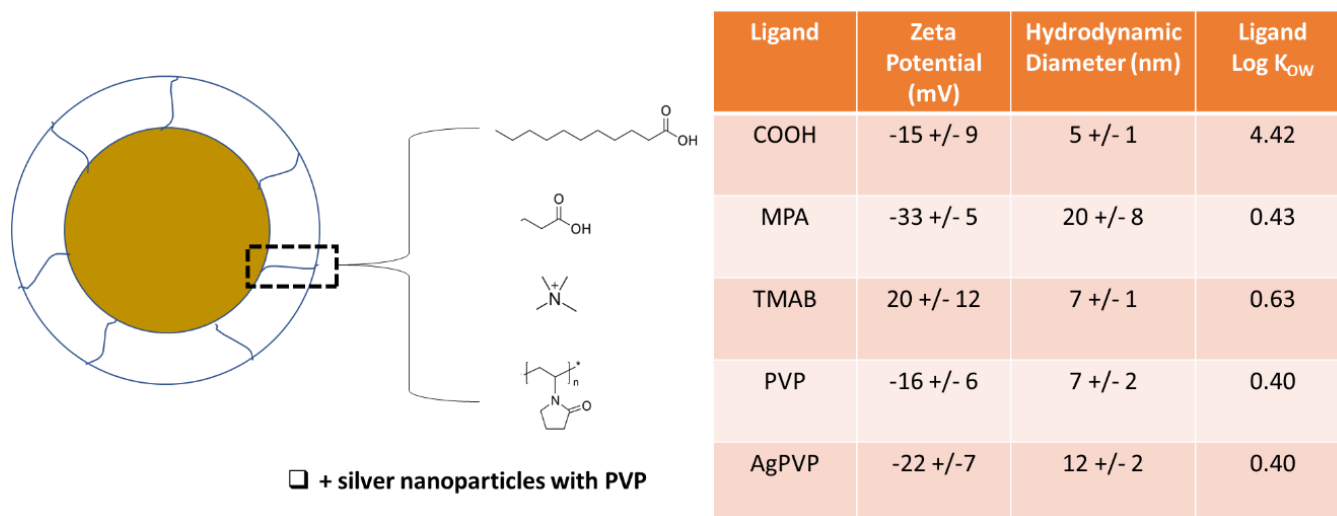


**Figure 7.** Summary of nanoparticles' characteristics. Measurements of the zeta potential and hydrodynamic diameter were done using Malvern Zetasizer (Malvern Panalytical, UK). Solutions of purified NPs were first diluted with ddH<sub>2</sub>O (1:5), run through 0.4  $\mu$ m filters, and then added to folded capillary zeta cells (Malvern Panalytical, UK) to perform the analysis. Log  $K_{ow}$  values were obtained from (Saha et al., 2013).

### The Effect of NPs and Colchicine

Because of possible aggregation of NPs in solution, it is essential to examine multiple concentrations, especially since a mechanistic investigation that examines whether NPs act on the membrane is performed. MANCOVA accounts for the variation in concentration but requires the assumption of linear responses to changes in concentration and parallel slopes for each level of the independent variables. Nevertheless, slopes of the concentration effect across NPs are not parallel and there is an interaction between concentration and NP type. Thus, MANCOVA is not possible, and the data are split into 3 datasets where a 2-way MANOVA is done on each.

For the first concentration (10 nM), univariate assumptions were first tested. Levene's test indicated that both dependent variables have homogenous variances with p-values of 0.821 and 0.438 for hemolysis and deformability, respectively. Box's M-test for homogeneity indicated

that data also pass homogeneity of covariance matrices with a p-value of 0.25. Shapiro-wilk test indicated that both dependent variables pass normality with p-values of 0.764 and 0.287 for hemolysis and deformability, respectively. Moreover, data pass multivariate normality with a p-value of 0.239 for multivariate Shapiro-Wilk normality test. MANOVA was run on the data from this concentration and the results are summarized in table 1. Clearly, we have a significant interaction between NP type and colchicine presence ( $p= 0.000975$  using Pillai's test). Yet, examination of figure 8 shows that the effect size of colchicine varies across NPs, but this effect is uniform causing an increase in hemolysis and a decrease in membrane deformability.

**Table 1.** Multivariate analysis of variance (MANOVA) on % hemolysis and deformability index data at 10 nM NP concentration.

		value	F	df1	df2	p
NP	Pillai's Trace	1.1961979	7.440873	8	40	0.0000050
inhibitor	Pillai's Trace	0.9607987	232.839196	2	19	< .0000001
NP:inhibitor	Pillai's Trace	0.9155369	4.221152	8	40	0.0009746

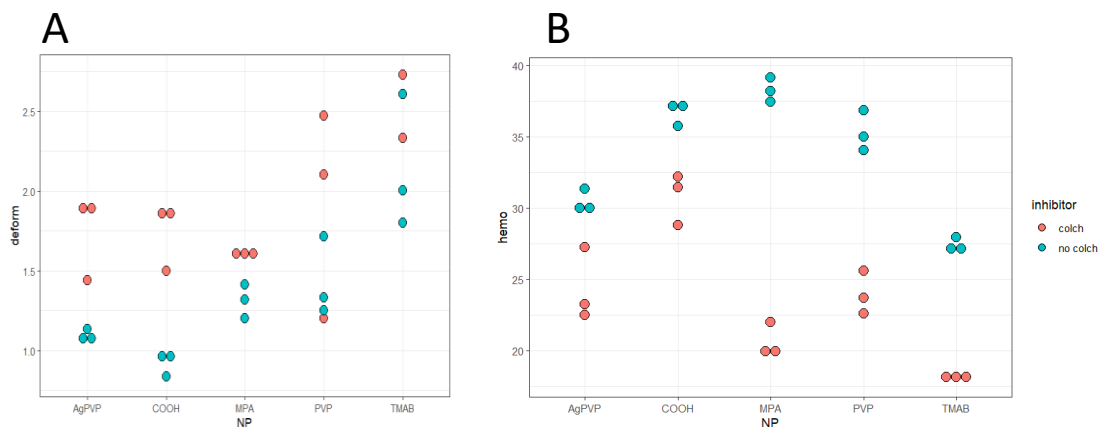


**Figure 8.** Raw plots of deformability index and % hemolysis data at 10 nM NP concentration. A) represents the deformability index ( $\text{mL}\cdot\text{min}^{-1}$ ) of RBCs in response to all NPs with and without colchicine. B) represents % hemolysis of RBCs in response to all NPs with and without colchicine. Data were plotted with RStudio (2023).

The MANOVA was followed by pairwise comparisons using permutational MANOVAs. The results are summarized in table 2, where significantly different comparisons were assessed using Benjamini-Hochberg correction and a false discovery rate of 20%. This large false discovery rate is appropriate here because the nature of MANOVA is exploratory. As shown in table 2, NPs with COOH ligand are significantly different from those with TMAB and the control NP AgPVP. Also, NPs with MPA are significantly different from TMAB NPs. The effect of colchicine in each NP was also investigated and the results are summarized in table 3. Here, the test used is Hotelling's t-test with a corrected alpha level of  $\alpha=0.01$  (Bonferroni correction). The results indicate that colchicine does not significantly affect gold NPs with COOH or AgPVP NPs.

**Table 2.** Permutational pairwise comparisons on the multivariate effect of NP types. Significant p-values with Benjamini-Hochberg correction are indicated with an asterisk.

<b>Comparison</b>	<b>P-value</b>
COOH vs AgPVP	0.010*
COOH vs MPA	0.687
COOH vs PVP	0.599
COOH vs TMAB	0.020*
MPA vs AgPVP	0.757
MPA vs PVP	0.687
MPA vs TMAB	0.023*
PVP vs AgPVP	0.523
PVP vs TMAB	0.226
AgPVP vs TMAB	0.120

**Table 3.** Hotelling's t-test results on the effect of colchicine in each NP type. The corrected alpha level is 0.01 and the significant differences are indicated with an asterisk.

<b>Effect of Colchicine on</b>	<b>P-value</b>
COOH	0.025
MPA	0.00078*
PVP	0.0034*
AgPVP	0.017
TMAB	0.00018*

Before doing the univariate analysis, canonical discriminant analysis was performed to understand the relationship between the dependent variables. Figure 9 shows how the dependent variables correlate for NP types and colchicine presence. Clearly there is negative correlation in the canonical analysis of NP types with standardized canonical coefficients of 0.972 and -0.470 in the eigen vector that explains 97% of variation for hemolysis and deformability, respectively. Similar correlation is observed in the canonical analysis of colchicine presence with standardized canonical coefficients of 0.999 and -0.367 for hemolysis and deformability, respectively.

Finally, a two-way ANOVA with Tukey HSD post hoc analysis was performed on each dependent variable. For hemolysis analysis, there is a significant interaction between NP type and colchicine presence ( $p=0.00000106$ ), and only post hoc analysis is used to interpret the results. Whereas for deformability analysis, there is no significant interaction ( $p=0.395$ ). Therefore, the effect of NP type ( $p=0.000734$ ) and colchicine ( $p=0.000528$ ) are significant. As shown in figure 10A, TMAB and AgPVP NPs cause significantly less hemolysis in the absence of colchicine, whereas COOH NPs cause significantly larger hemolysis than other NPs in the presence of colchicine. For membrane deformability results in figure 10B, colchicine increased membrane deformability significantly in all NPs, whereas TMAB NPs caused a significantly larger index (less toxicity) compared to other NPs.

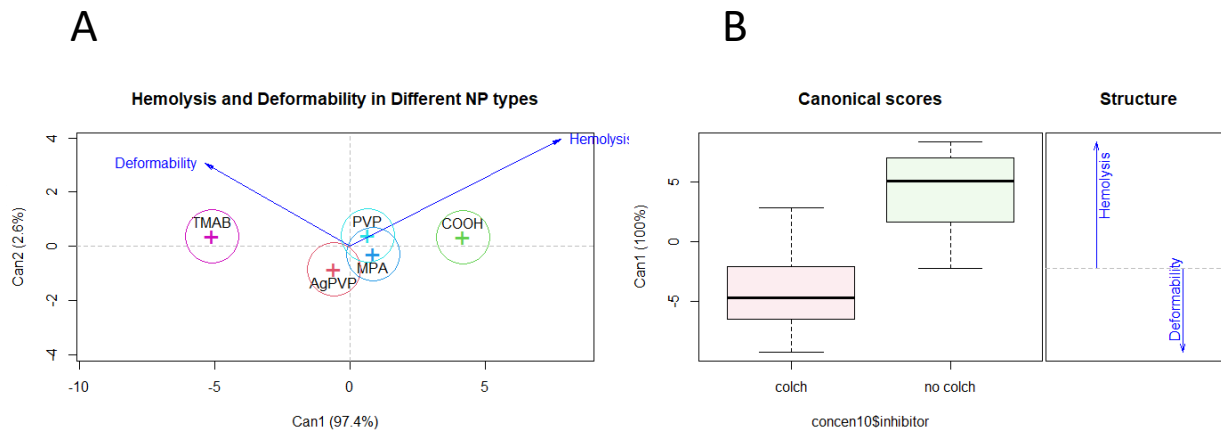


**Figure 9.** Canonical discriminant analysis of the MANOVA on the deformability index and % hemolysis data at 10 nM NP concentration. A) illustrates the negative correlation between the deformability index and % hemolysis and the contribution to the variation made by the different NPs. Can1 and Can2 represent two eigen vectors that explain 97% and 3 % of the statistical variation, respectively. B) illustrates the effect of colchicine on the deformability index and % hemolysis and the negative correlation between these two dependent variables.

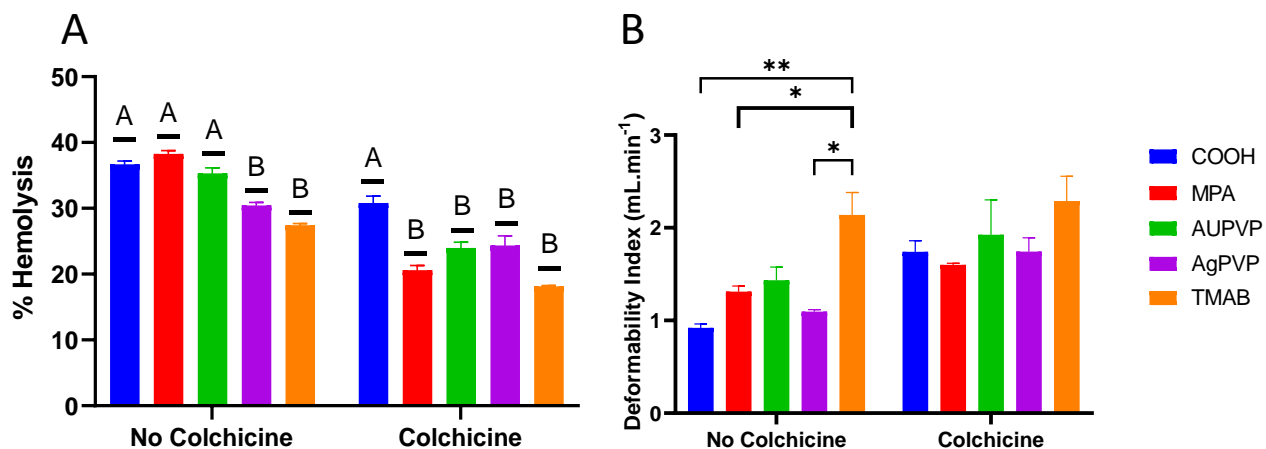


**Figure 10.** Bar graph of the effect of NPs (gold nanoparticles attached with undecanoic acid (COOH), mercaptopropionic acid (MPA), polyvinylpyrrolidone (PVP), and trimethyl ammonium bromide (TMAB); and commercially obtained silver nanoparticles of the same core size (5nm) and ligated with PVP (AgPVP)) and colchicine on the deformability index and % hemolysis of RBCs. A) represent the results of % hemolysis. Tukey HSD test was used for the post hoc analysis. Different letters within a single colchicine level differ significantly and the effect of colchicine is significant in all NPs. B) represents the results of membrane deformability. The effect of colchicine was assessed before the post hoc analysis (no interaction) and found to be significant in all NPs ( $p = 0.0005281$ ). Significant differences in each colchicine level are labeled with asterisks (\*  $p < 0.05$ , \*\*  $p < 0.01$ , and \*\*\*  $p < 0.001$ ).

For the second concentration (20 nM), univariate assumptions were tested again. Levene’s test indicated that both dependent variables have homogenous variances with p-values of 0.805 and 0.751 for hemolysis and deformability, respectively. Box’s M-test indicated that data also pass homogeneity of covariance matrices with a p-value of 0.207. Shapiro-wilk test indicated that both dependent variables pass normality with p-values of 0.605 and 0.672 for hemolysis and deformability, respectively. Nonetheless, data did not pass multivariate normality with a p-value of 0.0130 for multivariate Shapiro-Wilk normality test. MANOVA was run on the data from this concentration and the results are summarized in table 4. Clearly, we have a significant interaction between NP type and colchicine presence ( $p= 0.000975$  using Pillai’s test). As in the first concentration, examination of figure 11 shows that the effect size of colchicine varies across NPs but this effect is uniform causing an increase in hemolysis and a decrease in membrane deformability.

**Table 4.** Multivariate analysis of variance (MANOVA) on % hemolysis and deformability index data at 20 nM NP concentration.

		value	F	df1	df2	p
NP	Pillai's Trace	1.1893593	7.335922	8	40	0.0000059
inhibitor	Pillai's Trace	0.9443298	161.147914	2	19	< .0000001
NP:inhibitor	Pillai's Trace	1.2793848	8.877031	8	40	0.0000007

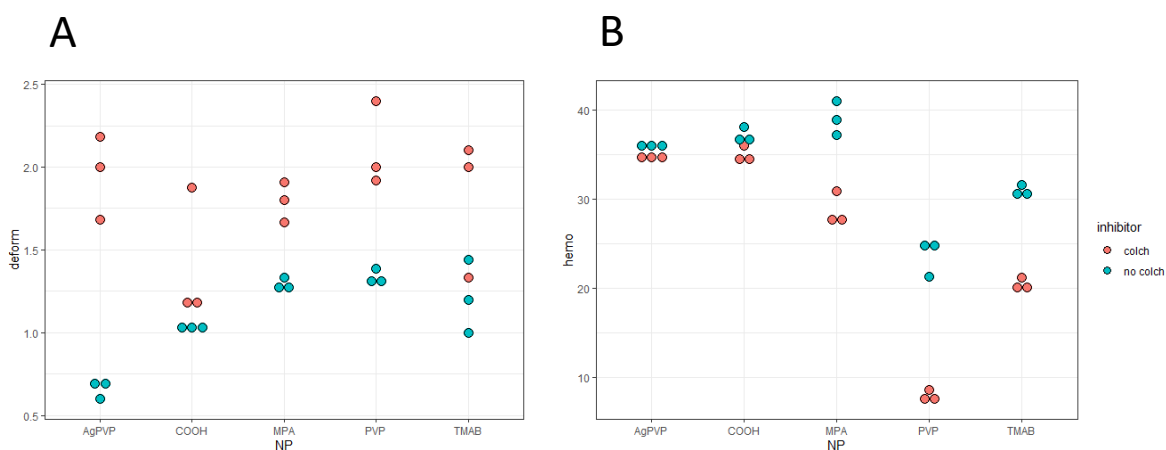


**Figure 11.** Raw plots of deformability index and % hemolysis data at 20 nM NP concentration. A) represents the deformability index ( $\text{mL}\cdot\text{min}^{-1}$ ) of RBCs in response to all NPs with and without colchicine. B) represents % hemolysis of RBCs in response to all NPs with and without colchicine. Data were plotted with RStudio (2023).

The MANOVA was followed by pairwise comparisons using permutational MANOVAs. The results are summarized in table 5, where significantly different comparisons were assessed using Benjamini-Hochberg correction and a false discovery rate of 20%. It has become clearer how concentration interacts with NP type. Responses to the different NPs became significantly different between all NPs except for between COOH, MPA, and AgPVP NPs. This indicates that responses to AgPVP and PVP became different than in the first concentration. A comparison between figure 5 and figure 3 shows how AgPVP became more toxic and PVP became less toxic. The effect of colchicine in each NP was also investigated and the results are summarized in table 6. Because data failed multivariate normality, Hotelling's t-test on the effect of colchicine is permuted with a corrected alpha level of  $\alpha=0.01$ . The results indicate that colchicine affects all NPs significantly and figure 11 shows that colchicine is causing NPs to be less toxic.

**Table 5.** Permutational pairwise comparisons on the multivariate effect of NP types at 20 nM. Significant p-values with Benjamini-Hochberg correction (FDR=20%) are indicated with an asterisk.

Comparison	P-value
COOH vs AgPVP	0.606
COOH vs MPA	0.318
COOH vs PVP	0.0067*
COOH vs TMAB	0.0067*
MPA vs AgPVP	0.748
MPA vs PVP	0.0067*
MPA vs TMAB	0.0160*
PVP vs AgPVP	0.0125*
PVP vs TMAB	0.0614*
AgPVP vs TMAB	0.0217*

**Table 6.** Permutational Hotelling's t-test results on the effect of colchicine in each NP type. The corrected alpha level is 0.01 and the significant differences are indicated with an asterisk.

Effect of Colchicine on	P-value
COOH	~0*
MPA	~0*
PVP	~0*
AgPVP	~0*
TMAB	~0*

The canonical discriminant analysis at this concentration is shown in figure 12 where the correlation between hemolysis and deformability is revealed for NP types and colchicine presence. Again, there is negative correlation in the canonical analysis of NP types with standardized canonical coefficients of 1.05 and -0.232 in the eigen vector that explains 99% of

variation for hemolysis and deformability, respectively. Similar correlation is observed in the canonical analysis of colchicine presence with standardized canonical coefficients of 0.937 and -0.161 for hemolysis and deformability, respectively.

Finally, a two-way ANOVA with Tukey HSD post hoc analysis was performed on each dependent variable. For hemolysis analysis, there is a significant interaction between NP type and colchicine presence ( $p=0.00000000324$ ), and only post hoc analysis is used to interpret the results. Also, deformability analysis indicated there is a significant interaction ( $p=0.0256$ ) and only Tukey HSD tests are used to draw conclusions. As shown in figure 13A, TMAB and PVP NPs cause significantly less hemolysis than other NPs regardless of colchicine presence. Whereas MPA NPs-induced hemolysis drops in the presence of colchicine but remains significantly higher than PVP and TMAB. For membrane deformability results in figure 13B, colchicine increased membrane deformability in all NPs, but significant increases only occur in PVP and AgPVP.

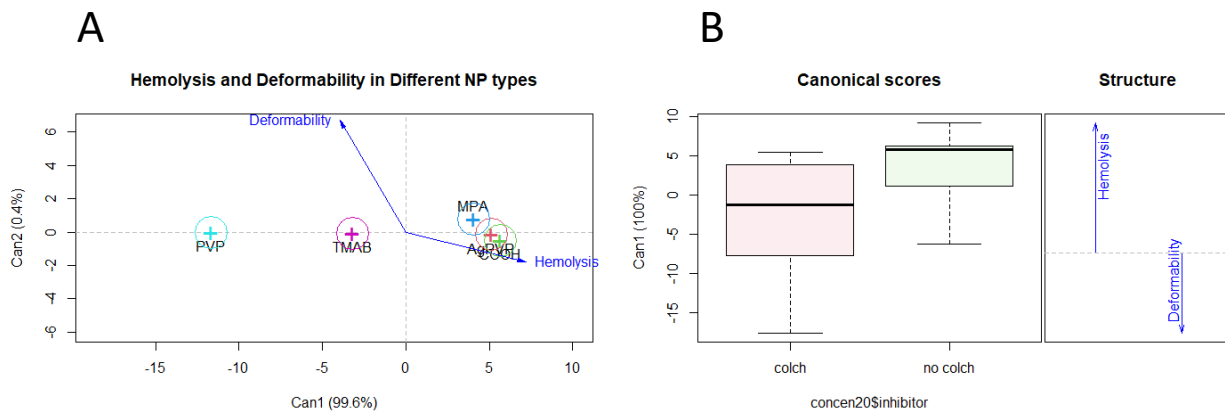


**Figure 12.** Canonical discriminant analysis of the MANOVA on the deformability index and % hemolysis data at 20 nM NP concentration. A) illustrates the negative correlation between the deformability index and % hemolysis and the contribution to the variation made by the different NPs. Can1 and Can2 represent two eigen vectors that explain 99.6% and 0.4 % of the statistical variation, respectively. B) illustrates the effect of colchicine on the deformability index and % hemolysis and the negative correlation between these two dependent variables.

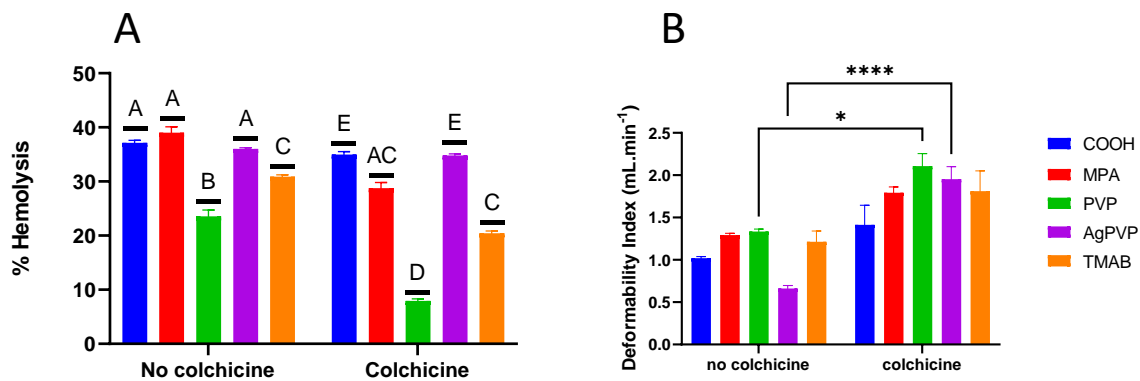


**Figure 13.** Bar graph of the effect of NPs (gold nanoparticles attached with undecanoic acid (COOH), mercaptopropionic acid (MPA), polyvinylpyrrolidone (PVP), and trimethyl ammonium bromide (TMAB); and commercially obtained silver nanoparticles of the same core size (5nm) and ligated with PVP (AgPVP)) and colchicine on the deformability index and % hemolysis of RBCs. A) represent the results of % hemolysis. Tukey HSD test was used for the post hoc analysis. Different letters within a single colchicine level differ significantly and the effect of colchicine is significant in all NPs. B) represents the results of membrane deformability. Tukey HSD test was used for the post hoc analysis. Significant differences are indicated with asterisks (\*  $p < 0.05$ , \*\* $p < 0.01$ , \*\*\* $p < 0.001$ , and \*\*\*\* $p < 0.0001$ ).

For the third concentration (40 nM), univariate assumptions were first tested. Levene's test indicated that both dependent variables have homogenous variances with p-values of 0.777 and 0.280 for hemolysis and deformability, respectively. Box's M-test for homogeneity indicated that data also pass homogeneity of covariance matrices with a p-value of 0.0435. Shapiro-wilk test indicated that the p-values are 0.0101 and 0.771 for hemolysis and deformability, respectively. Because univariate normality was not passed for deformability data, log 10 transformation was done on them. The Shapiro-wilk test indicated that log 10 deformability passed normality with a p-value of 0.200. Levene's test indicated that log 10 deformability data passed homogeneity of variance with a p-value of 0.570. Box's M-test indicated that data also pass homogeneity of covariance matrices with a p-value of 0.136. Data did not pass multivariate

normality and the multivariate Shapiro-Wilk normality test showed a p-value of 0.0261.

MANOVA was run on the data from this concentration and the results are summarized in table 7.

Clearly, we have a significant interaction between NP type and colchicine presence ( $p=0.00000157$  using Pillai's test). Again, examination of figure 14 shows that the effect size of colchicine varies across NPs but this effect is uniform causing an increase in hemolysis and a decrease in log 10 membrane deformability.

**Table 7.** Multivariate analysis of variance (MANOVA) on % hemolysis and deformability index data at 40 nM NP concentration.

		value	F	df1	df2	p
NP	Pillai's Trace	1.4528620	13.276923	8	40	< .0000001
inhibitor	Pillai's Trace	0.9854188	642.023261	2	19	< .0000001
NP:inhibitor	Pillai's Trace	1.2461941	8.266015	8	40	0.0000016

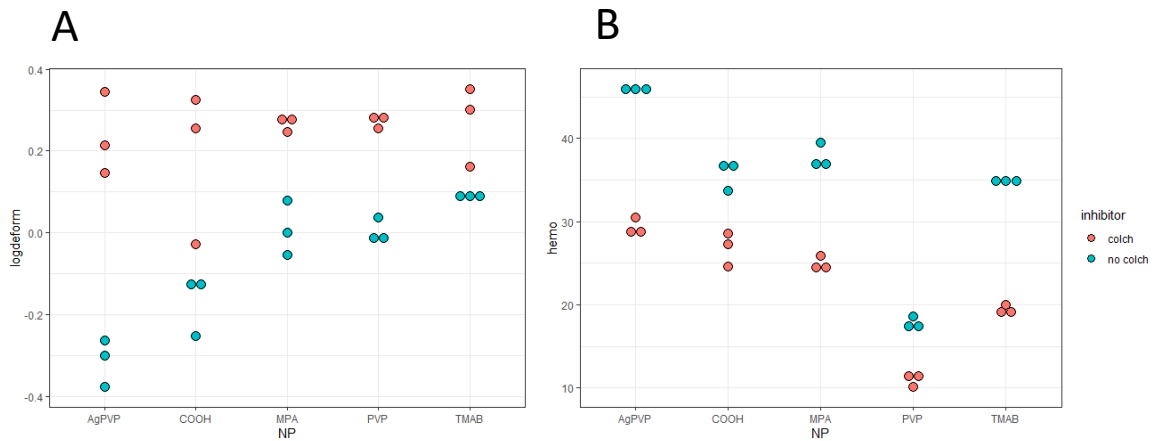


**Figure 14.** Raw plots of deformability index and % hemolysis data at 40 nM NP concentration. A) represents the log 10 deformability index ( $\text{mL}\cdot\text{min}^{-1}$ ) of RBCs in response to all NPs with and without colchicine. B) represents % hemolysis of RBCs in response to all NPs with and without colchicine. Data were plotted with RStudio (2023).

The MANOVA was followed by pairwise comparisons using permutational MANOVAs. The results are summarized in table 8, where significantly different comparisons were assessed using Benjamini-Hochberg correction and a false discovery rate of 20%. Again, the responses to PVP are significantly different than other NPs. The effect of colchicine in each NP was also investigated and the results are summarized in table 9. Because data failed multivariate normality, Hotelling's t-test on the effect of colchicine is permuted with a corrected alpha level of  $\alpha=0.01$ . The results indicate that colchicine affects all NPs significantly and figure 14 shows that colchicine is causing NPs to be less toxic.

**Table 8.** Permutational pairwise comparisons on the multivariate effect of NP types at 20 nM. Significant p-values with Benjamini-Hochberg correction (FDR=20%) are indicated with an asterisk.

Comparison	P-value
COOH vs AgPVP	0.212
COOH vs MPA	0.414
COOH vs PVP	0.005*
COOH vs TMAB	0.419
MPA vs AgPVP	0.508
MPA vs PVP	0.005*
MPA vs TMAB	0.649
PVP vs AgPVP	0.0067*
PVP vs TMAB	0.01*
AgPVP vs TMAB	0.303

**Table 9.** Permutational Hotelling’s t-test results on the effect of colchicine in each NP type. The corrected alpha level is 0.01 and the significant differences are indicated with an asterisk.

Effect of Colchicine on	P-value
COOH	~0*
MPA	~0*
PVP	~0*
AgPVP	~0*
TMAB	~0*

The canonical discriminant analysis at this concentration is shown in figure 15 where the correlation between hemolysis and deformability is revealed for NP types and colchicine presence. There is negative correlation in the canonical analysis of NP types with standardized canonical coefficients of 1.07 and -0.477 in the eigen vector that explains 99% of variation for hemolysis and deformability, respectively. Similar correlation is observed in the canonical analysis of colchicine presence with standardized canonical coefficients of 1.03 and -0.658 for hemolysis and deformability, respectively.

Finally, a two-way ANOVA with Tukey HSD post hoc analysis was performed for each dependent variable. For hemolysis analysis, there is a significant interaction between NP type and colchicine presence ( $p=0.000000776$ ), and only post hoc analysis is used to interpret the results. Also, deformability analysis indicated there is a significant interaction ( $p=0.0119$ ). As shown in figure 16A, PVP NPs cause significantly less hemolysis than other NPs regardless of colchicine presence. Whereas AgPVP NPs cause larger hemolysis that is significantly higher than all NPs in the absence of colchicine but only significantly higher than TMAB and PVP NPs in the presence of colchicine. For membrane deformability results, figure 16B indicates that AgPVP NPs caused a significant decrease in deformability index relative to other NPs in the absence of colchicine. Whereas TMAB NPs had the least toxic effect causing the index to be

significantly higher relative to all other NPs. Colchicine increased membrane deformability in all NPs significantly except for in TMAB NPs.

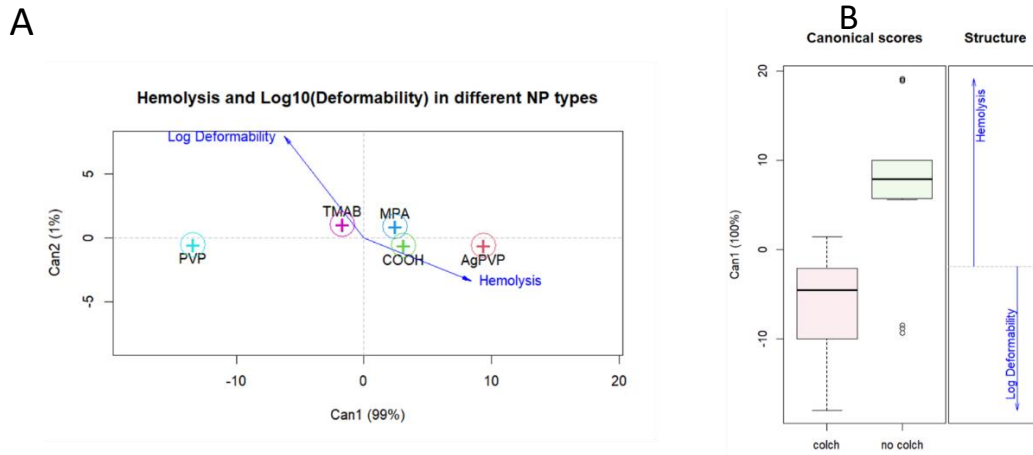


**Figure 15.** Canonical discriminant analysis of the MANOVA on the deformability index and % hemolysis data at 40 nM NP concentration. A) illustrates the negative correlation between the deformability index and % hemolysis and the contribution to the variation made by the different NPs. Can1 and Can2 represent two eigen vectors that explain 99% and 1 % of the statistical variation, respectively. B) illustrates the effect of colchicine on the deformability index and % hemolysis and the negative correlation between these two dependent variables.

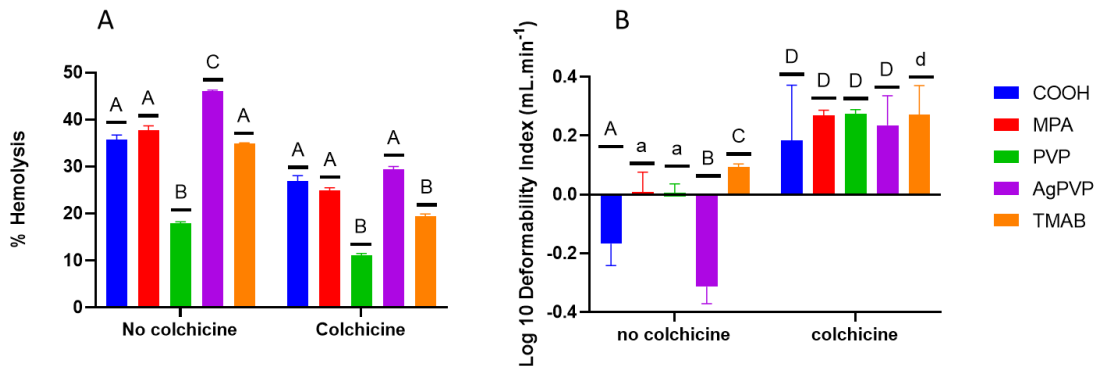


**Figure 16.** Bar graph of the effect of NPs (gold nanoparticles attached with undecanoic acid (COOH), mercaptopropionic acid (MPA), polyvinylpyrrolidone (PVP), and trimethyl ammonium bromide (TMAB); and commercially obtained silver nanoparticles of the same core size (5nm) and ligated with PVP (AgPVP)) and colchicine on the deformability index and % hemolysis of RBCs. A) represent the results of % hemolysis. Tukey HSD test was used for the post hoc analysis. Different letters within a single colchicine level differ significantly and the effect of colchicine is significant in all NPs. B) represents the results of membrane deformability. Significant differences using Tukey HSD in each colchicine level are indicated by the different letters. The effect of colchicine was assessed with Tukey HSD and found to be significant in all NPs except for TMAB.

## Discussion:

The approach we follow in interpreting the results is to examine the MANOVA in an exploratory manner and then make final conclusions with the separate ANOVAs. The exploratory nature of the MANOVA in this study aims to establish the relationship between hemolysis and deformability and identify which NPs contribute most to the variation.

### **MANOVA conclusions**

There is a significant interaction between NP type and colchicine presence at all NP concentrations. Thus, the conclusions can only be made with post hoc and canonical analyses. For 10 nM, as indicated in table 2, COOH NPs causes significantly larger toxicity than AgPVP and TMAB. Moreover, MPA NPs causes larger toxicity than TMAB. This suggests that the most hydrophobic ligand COOH causes the largest toxicity whereas the positively charged TMAB ligand is associated with smallest toxicity. Table 3 indicates that the effect of colchicine is not significant in the COOH NPs or in AgPVP, which suggests that COOH might be acting extracellularly. The insignificant effect of colchicine on AgPVP NPs might stem from the fact that AgPVP NPs cause their toxicity through the release of Ag<sup>+</sup>. However, colchicine protected RBCs from other NPs significantly by increasing the deformability index and decreasing hemolysis.

For 20 nM, as indicated in table 5, TMAB and PVP are significantly less toxic than MPA, COOH, and AgPVP. While TMAB complied with the previous pattern, the toxicity of PVP dropped significantly suggesting a huge aggregation of these NPs. Table 6 indicates that the effect of colchicine is prominent in all NPs. This is probably because as NPs aggregate, they tend to be engulfed by the cells (L. Q. Chen et al., 2015) and colchicine blocked this engulfment. It is

noticeable how AgPVP NPs caused toxicity similar to COOH and MPA which confirms that these NPs release toxic  $\text{Ag}^+$  in a concentration dependent manner (Huang et al., 2016). For 40 nM, as indicated in table 7, PVP NPs are significantly less toxic than all NPs. TMAB still complied with the previous pattern, but it showed increased toxicity relative to the previous concentration. Table 8 indicates that the effect of colchicine is prominent in all NPs as in 20 nM. Again, this is probably because colchicine blocked the engulfment of aggregated NPs. Thus, colchicine protected RBCs by increasing the deformability index and decreasing hemolysis. AgPVP NPs caused the largest toxicity, although not significant, confirming again their concentration-dependent toxicity.

In summary MANOVA revealed that hemolysis and deformability negatively correlate which suggests that NPs at least partially cause hemolysis through membrane interaction (reduced membrane deformability). In addition, increasing the hydrophobicity of the ligand increases toxicity with positively charged TMAB being the least toxic. The effect of colchicine is protective as it decreases hemolysis and increases membrane deformability significantly in all NPs except for COOH and AgPVP at 10 nM.

### **ANOVA conclusions**

After obtaining the significant MANOVA we conducted two ANOVAs each corresponding to a dependent variable at each concentration. The conclusions that will be made are not exploratory and thus the conservative Tukey HSD tests were used.

For 10 nM, figure 10 indicates that TMAB and AgPVP cause significantly less hemolysis than other NPs in the absence of colchicine. In the presence of colchicine, COOH NPs cause significantly larger hemolysis than other NPs. This suggests that when acting extracellular

increasing the hydrophobicity increases hemolysis as established previously (Saha et al., 2013). Colchicine decreased hemolysis in all nanoparticles significantly, which suggests that all NPs induce their toxicity intracellularly at least partially. In the absence of colchicine, TMAB had significantly larger membrane deformability and thus lower toxicity than the other NPs. This confirms that positively charged NPs are causing less overall toxicity. Colchicine increased membrane deformability significantly which was not expected if NPs interacted with the membrane extracellular. Therefore, the interaction with the membrane might be through indirect mechanisms like lipid peroxidation.

For 20 nM, figure 13 indicates that TMAB and PVP cause significantly less hemolysis than other NPs in the absence of colchicine. In the presence of colchicine, COOH and AgPVP NPs cause significantly larger hemolysis than other NPs. This confirms the previous results that when acting extracellular increasing the hydrophobicity increases hemolysis. Whereas AgPVP release their  $\text{Ag}^+$  and depend less on their uptake intracellularly. Colchicine decreased hemolysis in all nanoparticles significantly, which suggests that all NPs induce their toxicity intracellularly at least partially. Membrane deformability results were much harder to interpret as there was statistically significant interaction between NP type and colchicine presence. The only significant difference was in PVP and AgPVP NPs suggesting that colchicine largely protected the cells from their effects on the membrane. Whereas this protection was not seen in other NPs.

For 40 nM, figure 16 indicates that PVP causes significantly less hemolysis than other NPs in the absence of colchicine, whereas AgPVP caused the largest hemolysis. In the presence of colchicine, PVP and TMAB NPs cause significantly less hemolysis than other NPs. Again, we notice the concentration-dependent AgPVP toxicity, the aggregation of PVP that decreases its hemolysis, and the less toxicity induced by the positive charge on TMAB. Colchicine decreased

hemolysis in all nanoparticles significantly, which suggests that all NPs induce their toxicity intracellularly at least partially. The same pattern is seen in deformability where AgPVP and COOH NPs cause the largest decrease in the deformability index whereas TMAB had the least toxic effect on membrane deformability. It is important to note however, that PVP despite causing the least hemolysis did not cause the highest deformability index suggesting that NPs may cause their toxic effects to the membrane without affecting its ability to deform.

### **Biological interpretations and Future Directions**

The complex statistical results can be summarized into 3 main conclusions. These are the decreased toxicity in response to the positively charged TMAB NPs, the large toxicity induced by the most hydrophobic COOH NPs, and the protective role of colchicine against toxicity of NPs.

NPs functionalized with cationic ligands tend to cause more lysis and cytotoxicity than anionic ligands as they are more attracted to the negatively charged outer leaflet of cellular membranes (Goodman et al., 2004). TMAB NPs would therefore be expected to cause more hemolysis and less deformability than all other NPs in our study, yet this was not the case. The discrepancy might be stemming from the different cell models used. Goodman et al. (2004) examined the toxic effects of NPs on fibroblast-like Cos-1 cells, that show limited motility within culture plates. RBCs are drastically different and can be thought of as very large particles with zeta potential that accumulate specific charges on their surfaces as shown in figure 17. The cations that surround the RBC form a layer (Fernandes et al., 2011) that might attract NPs with a negative zeta potential and repel positively charged NPs. Such characteristics are not seen in Cos-1 cells that have limited motility and capacity to form ionic layers. Therefore, we

hypothesize that TMAB NPs were deterred by this layer of ions whereas other NPs were attracted.

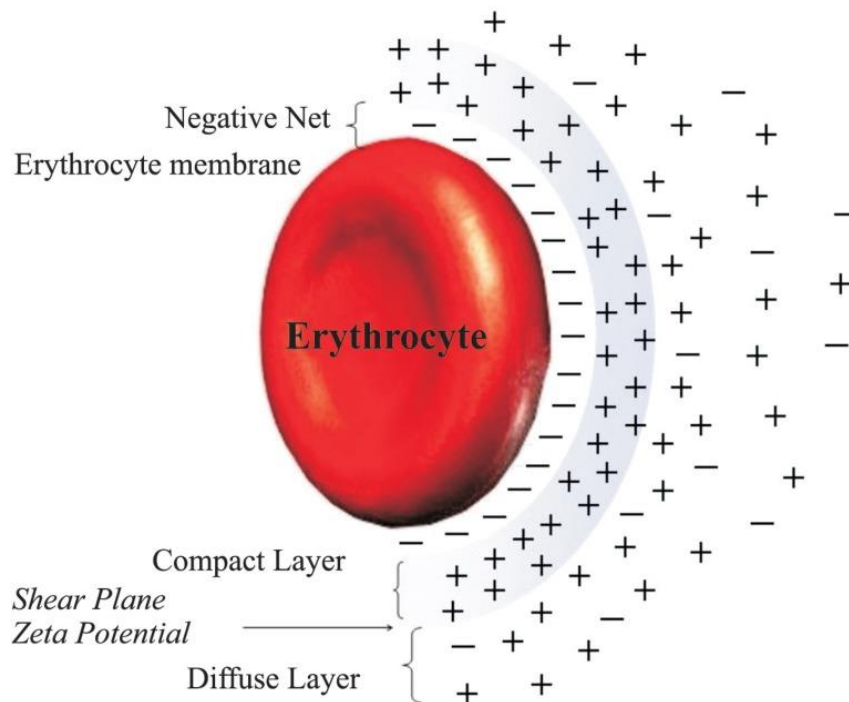


**Figure 17.** The electrical properties of circulating red blood cells. Image adopted from (Fernandes et al., 2011).

When NPs pass the cationic layer, their toxicity becomes dependent on the hydrophobicity of the ligand that mediates the interaction with the membrane and or cellular uptake. This has been previously investigated in detail using various ligands (Saha et al., 2013). Although this is also noticed in our study where COOH NPs cause the largest toxicity and seem to be less affected by colchicine compared to other NPs, final conclusions are hard to draw, especially since the ligands used beside COOH have similar hydrophobicities. Nevertheless, the hypothesis of increased toxicity in response to increased ligand hydrophobicity is still supported based on the results of COOH NPs.

The main gap in knowledge in the study was whether small gold NPs induce cytotoxicity solely through pore formation and interaction with the membranes. The negative correlation between hemolysis and membrane deformability indicates that the small gold NPs used in this study interact with the membrane in a detrimental manner that might at least partially cause hemolysis. The addition of colchicine rescued the cells from the decreased membrane deformability in many instances, which suggests that NPs cause membrane damage intracellularly. The results are further confirmed by the protective role colchicine plays in decreasing hemolysis in all NPs across all concentrations. One might argue that colchicine increased the extracellular osmolarity and thus decreased the osmotic pressure RBCs are experiencing. But colchicine has a log  $K_{ow}$  of 1.03 (Martin, 1996) partitioning almost equally between the cell and the extracellular solution although it slightly favours the partitioning towards the plasma membrane.

For future studies, it is essential to examine lipid peroxidation and other intracellular membrane-damaging pathways in response to NP exposure. This would further enhance our understanding of how NPs are causing increased hemolysis and decreased membrane deformability intracellularly. It is also suggested to test different endocytosis inhibitors to confirm the results are not colchicine specific and identify the specific endocytosis pathway behind the uptake of NPs. If NPs are to be used in biomedicine and their damage is mediated by their uptake, it could be beneficial to add endocytosis blockers during the period of NP exposure. Moreover, adding a blocker to a specific endocytosis pathway is less toxic to biological systems than blocking endocytosis nonspecifically as in the case of colchicine.

The study also highlights some points for future nanotoxicity experiments. For the first time, hemolysis and deformability are combined in a single analysis to understand their

correlation. This conveys much more information than studying each variable independently. What would be even more informative is using NPs with more variety in hydrophobicity and zeta potential values. Then, a MANOVA can examine how hemolysis and deformability vectors load on the axes explaining the variation in hydrophobicity and charge. In other words, the axes in MANOVA canonical analyses can be manually edited to represent charge and hydrophobicity or one could perform a principal component analysis (PCA) with the latter being less pleasant if parametric statistical assumptions are not met.

Also, this study provides a new experimental approach to examine the mechanisms of nanotoxicity. Previous researchers often used large concentrations of NPs, especially when examining the effects of the least toxic gold NPs (Saha et al., 2013). Here, we report the use of small NP concentrations coupled to RBCs at the edge of osmotic collapse at 50 mM NaCl extracellular saline. Instead of making the NPs strong enough to induce toxicity, RBCs were made weak enough to be affected by small NP concentrations. Again, this design works the best for studies that try to identify the mechanisms of nanotoxicity, and not the safety of certain NPs.

Overall, by combining hemolysis, deformability, and blocked endocytosis, the picture of the nanotoxicity becomes clearer. Small gold NPs induce cytotoxicity intracellularly and damage the membrane at least partially by intracellular pathways. Moreover, uptake is thought to be affected by the hydrophobicity of the ligand attached to the nanoparticles.

## Acknowledgements:

Thanks to Dr. Tyson MacCormack for his valuable guidance and support throughout the year.

Dr. MacCormack is a special professor who has made impactful input into my research and writing skills throughout my years at Mount Allison University. Special thanks to Dr. Vicki Meli who encouraged me to do research at the university and co-supervised the project.

I also would like to thank Samuel Patrick McGaw and Nir El for their help in collecting blood samples from fish.

I would like to acknowledge **R. P. Chapman** and **NSERC** for funding this project.

Thanks to Mount Allison University and the Department of Chemistry and Biochemistry for their support.

## References:

- Arai, T., & Okuyama, T. (1975). Fluorometric assay of tubulin-colchicine complex. *Analytical Biochemistry*, 69(2), 443–450. [https://doi.org/10.1016/0003-2697\(75\)90146-3](https://doi.org/10.1016/0003-2697(75)90146-3)
- Blair, H. A. (2018). Daunorubicin/Cytarabine Liposome: A Review in Acute Myeloid Leukaemia. *Drugs*, 78(18), 1903–1910. <https://doi.org/10.1007/s40265-018-1022-3>
- Carnovale, C., Bryant, G., Shukla, R., & Bansal, V. (2019). Identifying Trends in Gold Nanoparticle Toxicity and Uptake: Size, Shape, Capping Ligand, and Biological Corona. *ACS Omega*, 4(1), 242–256. <https://doi.org/10.1021/acsomega.8b03227>
- Chen, L. Q., Fang, L., Ling, J., Ding, C. Z., Kang, B., & Huang, C. Z. (2015). Nanotoxicity of Silver Nanoparticles to Red Blood Cells: Size Dependent Adsorption, Uptake, and Hemolytic Activity. *Chemical Research in Toxicology*, 28(3), 501–509. <https://doi.org/10.1021/tx500479m>
- Chen, X., & Schluesener, H. J. (2008). Nanosilver: A nanoparticle in medical application. *Toxicology Letters*, 176(1), 1–12. <https://doi.org/10.1016/j.toxlet.2007.10.004>
- Dalbeth, N., Lauterio, T. J., & Wolfe, H. R. (2014). Mechanism of Action of Colchicine in the Treatment of Gout. *Clinical Therapeutics*, 36(10), 1465–1479. <https://doi.org/10.1016/j.clinthera.2014.07.017>
- Dhyani, P., Quispe, C., Sharma, E., Bahukhandi, A., Sati, P., Attri, D. C., Szopa, A., Sharifi-Rad, J., Docea, A. O., Mardare, I., Calina, D., & Cho, W. C. (2022). Anticancer potential of alkaloids: A key emphasis to colchicine, vinblastine, vincristine, vindesine, vinorelbine and vincamine. *Cancer Cell International*, 22(1), 206. <https://doi.org/10.1186/s12935-022-02624-9>

- Drygin, Y. F., Blintsov, A. N., Osipov, A. P., Grigorenko, V. G., Andreeva, I. P., Uskov, A. I., Varitsev, Y. A., Anisimov, B. V., Novikov, V. K., & Atabekov, J. G. (2009). High-sensitivity express immunochromatographic method for detection of plant infection by tobacco mosaic virus. *Biochemistry*, *74*(9), 986–993. <https://doi.org/10.1134/S0006297909090065>
- Fernandes, H. P., Cesar, C. L., & Barjas-Castro, M. de L. (2011). Electrical properties of the red blood cell membrane and immunohematological investigation. *Revista Brasileira De Hematologia E Hemoterapia*, *33*(4), 297–301. <https://doi.org/10.5581/1516-8484.20110080>
- Ghanem, R., Baker, H., Seif, M. A., Al-Qawasmeh, R. A., Mataneh, A.-A., & Al-Gharabli, S. I. (2010). Photochemical Transformation of Colchicine: A Kinetic Study. *Journal of Solution Chemistry*, *39*(4), 441–456. <https://doi.org/10.1007/s10953-010-9515-z>
- Goodman, C. M., McCusker, C. D., Yilmaz, T., & Rotello, V. M. (2004). Toxicity of Gold Nanoparticles Functionalized with Cationic and Anionic Side Chains. *Bioconjugate Chemistry*, *15*(4), 897–900. <https://doi.org/10.1021/bc049951i>
- Green, M. R., Manikhas, G. M., Orlov, S., Afanasyev, B., Makhson, A. M., Bhar, P., & Hawkins, M. J. (2006). Abraxane®, a novel Cremophor®-free, albumin-bound particle form of paclitaxel for the treatment of advanced non-small-cell lung cancer. *Annals of Oncology*, *17*(8), 1263–1268. <https://doi.org/10.1093/annonc/mdl104>
- Haiss, W., Thanh, N. T. K., Aveyard, J., & Fernig, D. G. (2007). Determination of Size and Concentration of Gold Nanoparticles from UV–Vis Spectra. *Analytical Chemistry*, *79*(11), 4215–4221. <https://doi.org/10.1021/ac0702084>

- Hirsch, L. R., Stafford, R. J., Bankson, J. A., Sershen, S. R., Rivera, B., Price, R. E., Hazle, J. D., Halas, N. J., & West, J. L. (2003). Nanoshell-mediated near-infrared thermal therapy of tumors under magnetic resonance guidance. *Proceedings of the National Academy of Sciences*, *100*(23), 13549–13554. <https://doi.org/10.1073/pnas.2232479100>
- Hou, X., Zaks, T., Langer, R., & Dong, Y. (2021). Lipid nanoparticles for mRNA delivery. *Nature Reviews Materials*, *6*(12), Article 12. <https://doi.org/10.1038/s41578-021-00358-0>
- Huang, H., Lai, W., Cui, M., Liang, L., Lin, Y., Fang, Q., Liu, Y., & Xie, L. (2016). An Evaluation of Blood Compatibility of Silver Nanoparticles. *Scientific Reports*, *6*(1), Article 1. <https://doi.org/10.1038/srep25518>
- Jiang, J., Oberdörster, G., & Biswas, P. (2009). Characterization of size, surface charge, and agglomeration state of nanoparticle dispersions for toxicological studies. *Journal of Nanoparticle Research*, *11*(1), 77–89. <https://doi.org/10.1007/s11051-008-9446-4>
- Kitchens, K. M., Kolhatkar, R. B., Swaan, P. W., & Ghandehari, H. (2008). Endocytosis Inhibitors Prevent Poly(amidoamine) Dendrimer Internalization and Permeability across Caco-2 Cells. *Molecular Pharmaceutics*, *5*(2), 364–369. <https://doi.org/10.1021/mp700089s>
- Kruth, H. S., Jones, N. L., Huang, W., Zhao, B., Ishii, I., Chang, J., Combs, C. A., Malide, D., & Zhang, W.-Y. (2005). Macropinocytosis Is the Endocytic Pathway That Mediates Macrophage Foam Cell Formation with Native Low Density Lipoprotein\*. *Journal of Biological Chemistry*, *280*(3), 2352–2360. <https://doi.org/10.1074/jbc.M407167200>
- Lawrence, M. J., Raby, G. D., Teffer, A. K., Jeffries, K. M., Danylchuk, A. J., Eliason, E. J., Hasler, C. T., Clark, T. D., & Cooke, S. J. (2020). Best practices for non-lethal blood

- sampling of fish via the caudal vasculature. *Journal of Fish Biology*, 97(1), 4–15.  
<https://doi.org/10.1111/jfb.14339>
- Lin, I.-C., Liang, M., Liu, T.-Y., Monteiro, M. J., & Toth, I. (2012). Cellular transport pathways of polymer coated gold nanoparticles. *Nanomedicine: Nanotechnology, Biology and Medicine*, 8(1), 8–11. <https://doi.org/10.1016/j.nano.2011.09.014>
- Lin, Z.-Y., Kuo, C.-H., Wu, D.-C., & Chuang, W.-L. (2016). Anticancer effects of clinically acceptable colchicine concentrations on human gastric cancer cell lines. *The Kaohsiung Journal of Medical Sciences*, 32(2), 68–73. <https://doi.org/10.1016/j.kjms.2015.12.006>
- Martin, Y. C. (1996). Exploring QSAR: Hydrophobic, Electronic, and Steric Constants C. Hansch, A. Leo, and D. Hoekman. American Chemical Society, Washington, DC. 1995. Xix + 348 pp. 22 × 28.5 cm. Exploring QSAR: Fundamentals and Applications in Chemistry and Biology. C. Hansch and A. Leo. American Chemical Society, Washington, DC. 1995. Xvii + 557 pp. 18.5 × 26 cm. ISBN 0-8412-2993-7 (set). \$99.95 (set). *Journal of Medicinal Chemistry*, 39(5), 1189–1190.  
<https://doi.org/10.1021/jm950902o>
- Mateu Ferrando, R., Lay, L., & Polito, L. (2020). Gold nanoparticle-based platforms for vaccine development. *Drug Discovery Today: Technologies*, 38, 57–67.  
<https://doi.org/10.1016/j.ddtec.2021.02.001>
- Matovcik, L., Junga, I., & Schrier, S. (1985). Drug-induced endocytosis of neonatal erythrocytes. *Blood*, 65(5), 1056–1063. <https://doi.org/10.1182/blood.V65.5.1056.1056>
- McLeese, J. M., & Eales, J. G. (1996). 3,5,3'-Triiodo-L-thyronine and L-Thyroxine Uptake into Red Blood Cells of Rainbow Trout, *Oncorhynchus mykiss*. *General and Comparative Endocrinology*, 102(1), 47–55. <https://doi.org/10.1006/gcen.1996.0045>

- Mitchell, M. J., Billingsley, M. M., Haley, R. M., Wechsler, M. E., Peppas, N. A., & Langer, R. (2021). Engineering precision nanoparticles for drug delivery. *Nature Reviews Drug Discovery*, 20(2), Article 2. <https://doi.org/10.1038/s41573-020-0090-8>
- Mundy, D. I., Machleidt, T., Ying, Y., Anderson, R. G. W., & Bloom, G. S. (2002). Dual control of caveolar membrane traffic by microtubules and the actin cytoskeleton. *Journal of Cell Science*, 115(22), 4327–4339. <https://doi.org/10.1242/jcs.00117>
- Nash, G. B., & Egginton, S. (1993). Comparative rheology of human and trout red blood cells. *Journal of Experimental Biology*, 174(1), 109–122. <https://doi.org/10.1242/jeb.174.1.109>
- Nilsson, J., Ksiazek, T., & Thyberg, J. (1983). Effects of colchicine on DNA synthesis, endocytosis and fine structure of cultivated arterial smooth muscle cells. *Experimental Cell Research*, 143(2), 367–375. [https://doi.org/10.1016/0014-4827\(83\)90063-0](https://doi.org/10.1016/0014-4827(83)90063-0)
- Piasek, A., & Thyberg, J. (1979). Effects of colchicine on endocytosis and cellular inactivation of horseradish peroxidase in cultured chondrocytes. *Journal of Cell Biology*, 81(2), 426–437. <https://doi.org/10.1083/jcb.81.2.426>
- Qin, Z., Vijayaraman, S. B., Lin, H., Dai, Y., Zhao, L., Xie, J., Lin, W., Wu, Z., Li, J., & Lin, L. (2019). Antibacterial activity of erythrocyte from grass carp (*Ctenopharyngodon idella*) is associated with phagocytosis and reactive oxygen species generation. *Fish & Shellfish Immunology*, 92, 331–340. <https://doi.org/10.1016/j.fsi.2019.06.008>
- Rastinehad, A. R., Anastos, H., Wajswol, E., Winoker, J. S., Sfakianos, J. P., Doppalapudi, S. K., Carrick, M. R., Knauer, C. J., Taouli, B., Lewis, S. C., Tewari, A. K., Schwartz, J. A., Canfield, S. E., George, A. K., West, J. L., & Halas, N. J. (2019). Gold nanoshell-localized photothermal ablation of prostate tumors in a clinical pilot device study.

- Proceedings of the National Academy of Sciences*, 116(37), 18590–18596.  
<https://doi.org/10.1073/pnas.1906929116>
- Reid, H. L., Barnes, A. J., Lock, P. J., Dormandy, J. A., & Dormandy, T. L. (1976). A simple method for measuring erythrocyte deformability. *Journal of Clinical Pathology*, 29(9), 855–858. <https://doi.org/10.1136/jcp.29.9.855>
- Roiter, Y., Ornatska, M., Rammohan, A. R., Balakrishnan, J., Heine, D. R., & Minko, S. (2008). Interaction of Nanoparticles with Lipid Membrane. *Nano Letters*, 8(3), 941–944.  
<https://doi.org/10.1021/nl080080l>
- Rucareanu, S., Gandubert, V. J., & Lennox, R. B. (2006). 4-(N,N-Dimethylamino)pyridine-Protected Au Nanoparticles: Versatile Precursors for Water- and Organic-Soluble Gold Nanoparticles. *Chemistry of Materials*, 18(19), 4674–4680.  
<https://doi.org/10.1021/cm060793+>
- Saha, K., Moyano, D. F., & Rotello, V. M. (2013). Protein coronas suppress the hemolytic activity of hydrophilic and hydrophobic nanoparticles. *Materials Horizons*, 1(1), 102–105. <https://doi.org/10.1039/C3MH00075C>
- Stern, J. M., Kibanov Solomonov, V. V., Sazykina, E., Schwartz, J. A., Gad, S. C., & Goodrich, G. P. (2016). Initial Evaluation of the Safety of Nanoshell-Directed Photothermal Therapy in the Treatment of Prostate Disease. *International Journal of Toxicology*, 35(1), 38–46. <https://doi.org/10.1177/1091581815600170>
- Stosik, M., Tokarz-Deptuła, B., Deptuła, J., & Deptuła, W. (2020). Immune Functions of Erythrocytes in Osteichthyes. *Frontiers in Immunology*, 11.  
<https://www.frontiersin.org/articles/10.3389/fimmu.2020.01914>

- Suljević, D., & Mitrašinović-Brulić, M. (2020). The first record of brook trout (*Salvelinus fontinalis*, Salmonidae) blood cell characteristics and hematological profile: The influence of fish sex on leukocyte count. *Aquaculture International*, 28(6), 2505–2516. <https://doi.org/10.1007/s10499-020-00603-3>
- Tang, H., Chen, H., Jia, Y., Liu, X., Han, Z., Wang, A., Liu, Q., Li, X., & Feng, X. (2017). Effect of inhibitors of endocytosis and NF-κB signal pathway on folate-conjugated nanoparticle endocytosis by rat Kupffer cells. *International Journal of Nanomedicine*, 12, 6937–6947. <https://doi.org/10.2147/IJN.S141407>
- Yafout, M., Ousaid, A., Khayati, Y., & El Otmani, I. S. (2021). Gold nanoparticles as a drug delivery system for standard chemotherapeutics: A new lead for targeted pharmacological cancer treatments. *Scientific African*, 11, e00685. <https://doi.org/10.1016/j.sciaf.2020.e00685>
- Zhao, Y., Sun, X., Zhang, G., Trewyn, B. G., Slowing, I. I., & Lin, V. S.-Y. (2011). Interaction of Mesoporous Silica Nanoparticles with Human Red Blood Cell Membranes: Size and Surface Effects. *ACS Nano*, 5(2), 1366–1375. <https://doi.org/10.1021/nm103077k>

## Appendix:

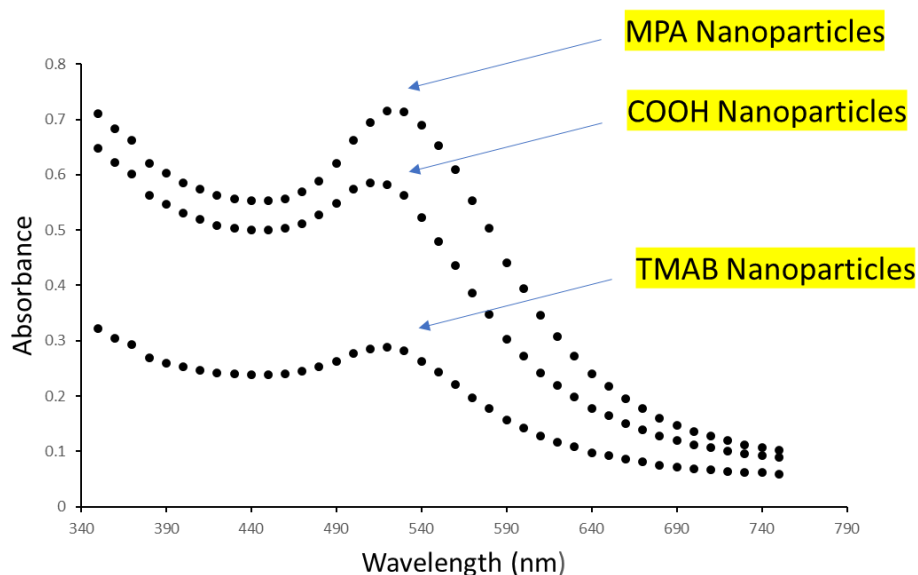


**Figure 1A.** Absorbance spectra of gold nanoparticles attached with undecanoic acid (COOH), mercaptopropionic acid (MPA), and trimethyl ammonium bromide (TMAB) ligands. The arrows point at the surface plasmon resonance peak. Solutions of NPs ( $V= 200 \mu\text{L}$ ) were added to a microplate and the absorbance spectra for each NP was determined using SpectraMax 190 (Molecular Devices, US). First, the wavelength at which surface plasmon resonance occurs was checked (should be around 520 nm for 5nm gold NPs).

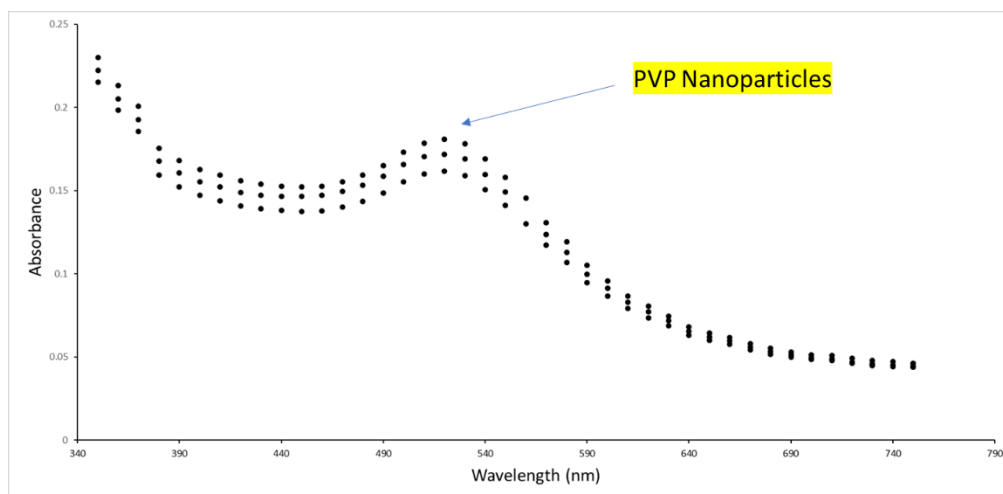


**Figure 2A.** Absorbance spectra of gold nanoparticles attached with polyvinylpyrrolidone (PVP). The arrow points at the surface plasmon resonance peak. Solutions of NPs ( $V= 200 \mu\text{L}$ ) were added to a microplate and the absorbance spectra for each NP was determined using SpectraMax 190 (Molecular Devices, US).

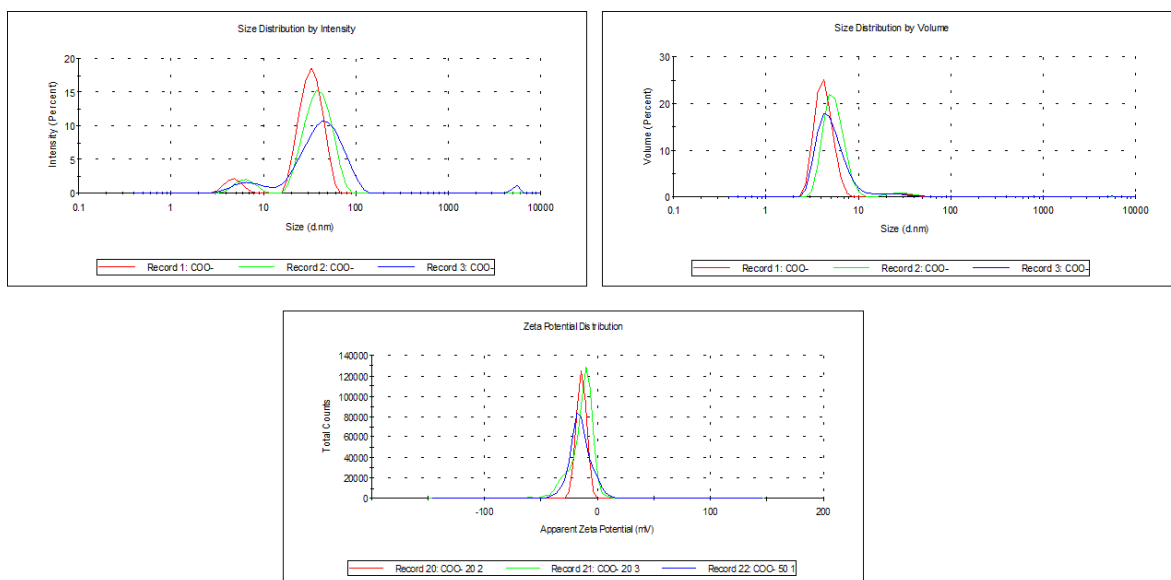


**Figure 3A.** Dynamic light scattering results of gold nanoparticles attached to undecanoic acid (COOH) ligands. Characterization of NPs was done using Malvern Zetasizer (Malvern Panalytical, UK). Solutions of purified NPs were first diluted with ddH<sub>2</sub>O (1:5), run through 0.4  $\mu$ m filters, and then added to folded capillary zeta cells (Malvern Panalytical, UK). Size results are shown on the top (distribution by intensity on the left and by volume on the right), and zeta potential results are on the bottom.

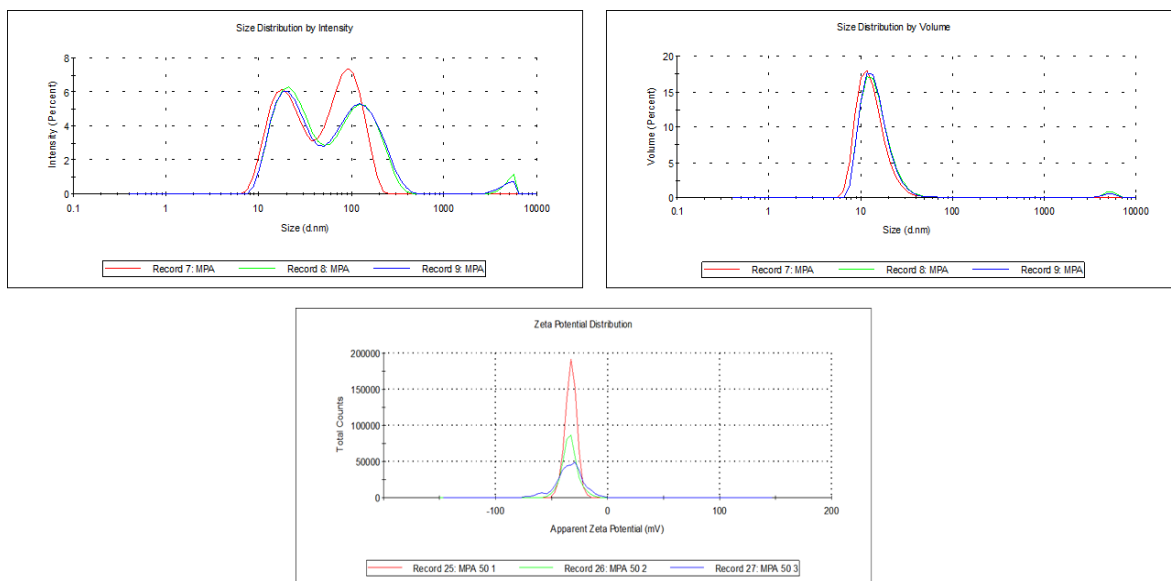


**Figure 4A.** Dynamic light scattering results of gold nanoparticles attached to mercaptopropionic acid (MPA) ligands. Solutions of purified NPs were first diluted with ddH<sub>2</sub>O (1:5), run through 0.4  $\mu$ m filters, and then added to folded capillary zeta cells (Malvern Panalytical, UK). Size results are shown on the top (distribution by intensity on the left and by volume on the right), and zeta potential results are on the bottom.

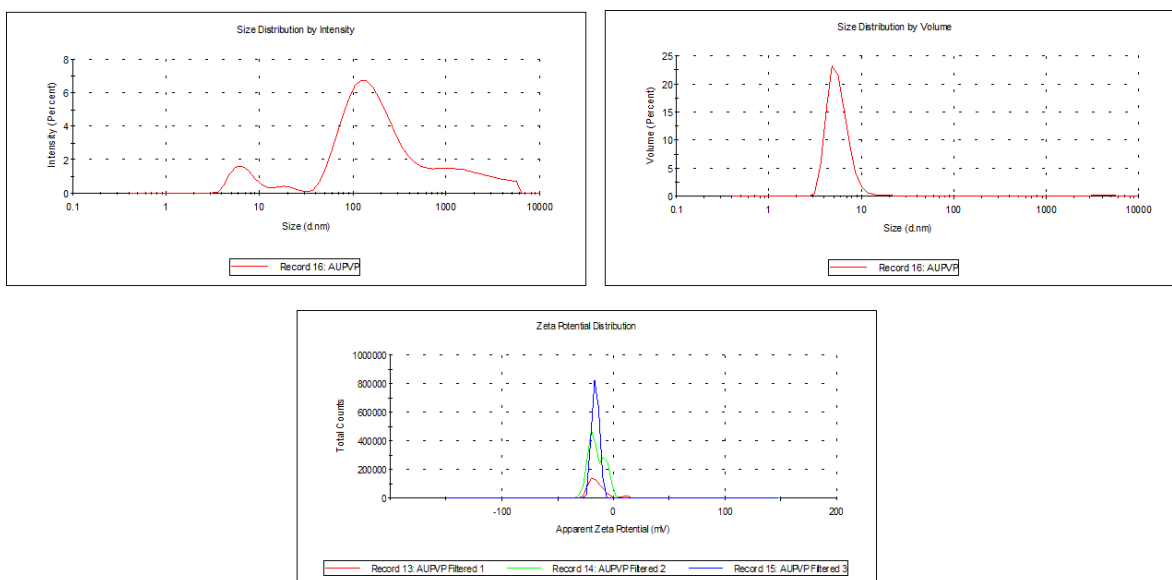


**Figure 5A.** Dynamic light scattering results of gold nanoparticles attached to polyvinylpyrrolidone (PVP) ligands. Solutions of purified NPs were first diluted with ddH<sub>2</sub>O (1:5), run through 0.4 μm filters, and then added to folded capillary zeta cells (Malvern Panalytical, UK). Size results are shown on the top (distribution by intensity on the left and by volume on the right), and zeta potential results are on the bottom.

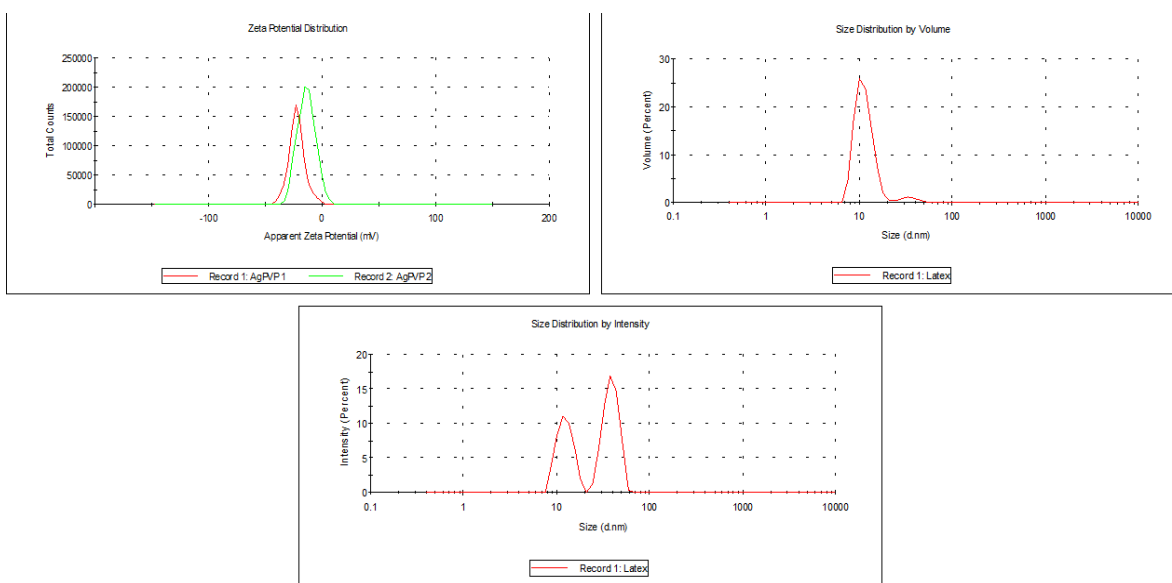


**Figure 6A.** Dynamic light scattering results of silver nanoparticles attached to polyvinylpyrrolidone (AgPVP) ligands. Solutions of purified NPs were first diluted with ddH<sub>2</sub>O (1:5), run through 0.4 μm filters, and then added to folded capillary zeta cells (Malvern Panalytical, UK). Size results are shown on the top (distribution by intensity on the left and by volume on the right), and zeta potential results are on the bottom.

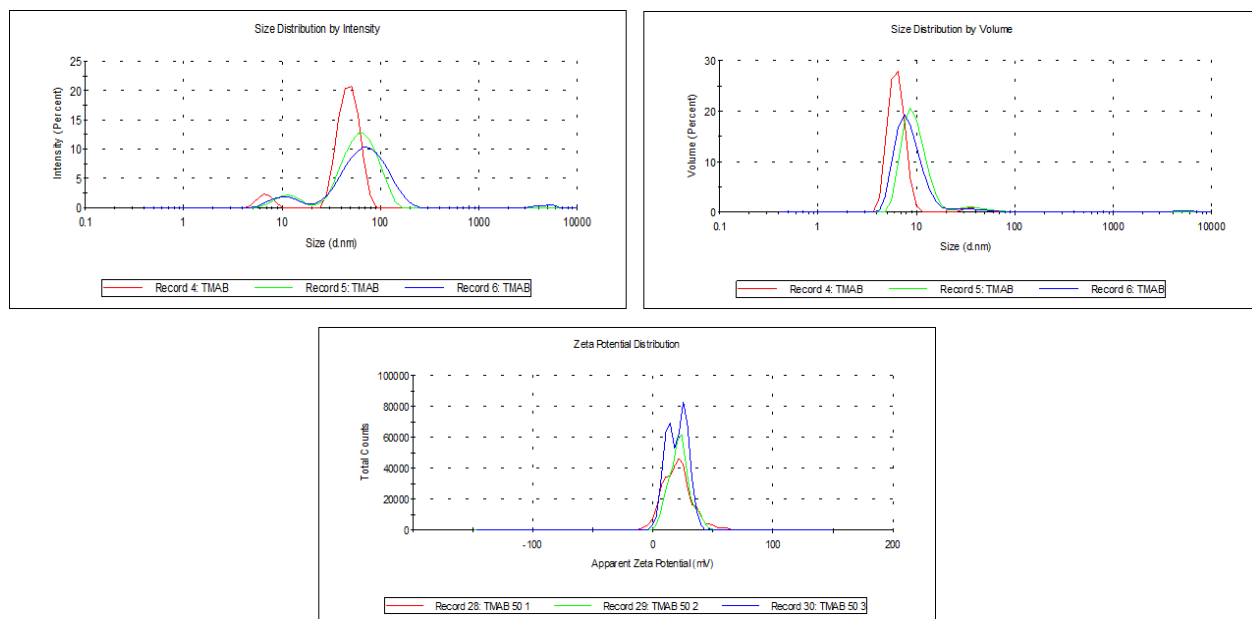


**Figure 7A.** Dynamic light scattering results of gold nanoparticles attached to trimethyl ammonium bromide (TMAB) ligands. Solutions of purified NPs were first diluted with ddH<sub>2</sub>O (1:5), run through 0.4  $\mu$ m filters, and then added to folded capillary zeta cells (Malvern Panalytical, UK). Size results are shown on the top (distribution by intensity on the left and by volume on the right), and zeta potential results are on the bottom.

**Table 1A.** Raw data of % hemolysis from equation 1 (after correcting for the absorbance of NPs at 570 nm) in response to the different nanoparticles and colchicine presence ([NaCl] = 50 mM).

NP type /C (nM)	%Hemolysis					
	NPs + RBC (-colchicine)			NPs + RBC (+colchicine)		
TMAB						
10	27.17528	27.9319	27.17528	17.96974	18.34805	18.15889
20	31.52585	30.76923	30.39092	21.18537	20.42875	19.67213
40	35.1198	34.93064	34.74149	20.05044	18.72636	19.67213
COOH						
10	37.26356	35.75032	37.0744	31.4628	28.81463	32.21942
20	36.88525	38.02018	36.50694	36.00252	34.67844	34.30013
40	36.88525	33.66961	36.50694	24.65322	28.62547	27.30139
MPA						
10	38.20933	39.15511	37.45271	22.00504	19.73518	20.11349
20	38.9029	40.98361	37.2005	30.83228	28.18411	27.23834
40	37.38966	36.44388	39.47037	25.91425	24.21185	24.77932
AuPVP						
10	36.88525	34.04792	34.99369	23.70744	25.59899	22.57251
20	32.97604	36.38083	36.56999	19.41992	19.23077	20.3657
40	18.60025	17.27617	17.65448	11.47541	10.15132	11.47541
AgPVP						
10	31.3367	30.01261	30.01261	22.50946	27.23834	23.26608
20	35.62421	36.38083	36.00252	34.17402	35.1198	35.1198
40	46.343	46.15385	45.58638	28.62547	29.00378	30.51702

**Table 2A.** Raw data of RBCs deformability index in response to the different nanoparticles and colchicine presence ([NaCl] = 143 mM).

	Deformability Index (mL.min <sup>-1</sup> )					
NP type / C (nM)	NPs + RBC (-colchicine)			NPs + RBC (+colchicine)		
TMAB						
10	2.6087	2.0040	1.8000	2.7273	2.3333	1.8000
20	1.2000	1.0000	1.4400	1.3333	2.1000	2.0000
40	1.2500	1.2000	1.2600	2.2500	2.0000	1.4483
COOH						
10	0.8372	0.9730	0.9500	1.8750	1.8462	1.5000
20	1.0000	1.0000	1.0588	1.1667	1.2000	1.8750
40	0.7500	0.7500	0.5581	0.9375	2.1176	1.8000
MPA						
10	1.4118	1.2000	1.3200	1.5789	1.6364	1.5789
20	1.2857	1.3333	1.2600	1.6667	1.9091	1.8000
40	0.8824	1.0000	1.2000	1.8750	1.9200	1.7647
AuPVP						
10	1.7143	1.2500	1.3333	2.4706	2.1000	1.2000
20	1.3846	1.3333	1.2857	2.4000	2.0000	1.9200
40	1.0909	1.0000	0.9474	1.9200	1.9091	1.8000
AgPVP						
10	1.0909	1.1351	1.0560	1.8750	1.9091	1.4400
20	0.6667	0.6000	0.7200	2.0000	2.1818	1.6800
40	0.5455	0.5000	0.4200	2.2105	1.6364	1.4000